Electronic Supplementary Information

Ultrafast Energy Transfer in a Pd(II)-Bridged Bisporphyrin Dyad

Mohammed Abdelhameed, Adam Langlois, Paul-Ludovic Karsenti, Sébastien Richeter, Romain Ruppert and Pierre D. Harvey

Table of Contents:

Comment [SR]: Remis en forme

Comment [SR]: Remis en forme

Experimental Section

Materials. The synthesis of the porphyrins **[Fb]** and **[Zn]**, and homo-dimers **[Fb-Fb]** and **[Zn-Zn]** was described earlier.[1] The reactions were performed under argon using oven-dried glassware and Schlenk techniques. Palladium acetate was purchased from Alfa Aesar. Dry toluene was obtained by distillation over Na/benzophenone. Preparative separations were performed by silica gel flash column chromatography (Merck SI 60, 40-63 μm). Dichloromethane (distilled over CaH_2) and cyclohexane used as eluents were obtained from Aldrich. ^1H and $^{13}C\{^1H\}$ NMR spectra were recorded in $CDCl_3$ on Bruker Avance 400 or 500 MHz spectrometer. ^1H and $^{13}C\{1H\}$ NMR spectra were calibrated to TMS on the basis of the relative chemical shift of the solvent as an internal standard. Abbreviations for ^1H NMR spectra used are as follows: s, singlet; d, doublet. UV-visible absorption spectra were recorded in $CHCl_3$ with an Agilent diode-array UV-visible spectrophotometer HP 8453. ESI mass spectra were recorded on a Bruker MicroTOF spectrometer.

***Synthesis of dyad* [Fb-Zn], *Procedure A*.** A solution of the palladium complex **[Fb-Fb]** (25 mg, $1.2x10^{-5}$ mol) and $Zn(OAc)_2•2H_2O$ (3 mg, $1.3x10^{-5}$ mol) was prepared in a $CHCl_3/CH_3OH$ mixture (18/2 mL) and degassed with argon. Then, the reaction mixture was stirred for 2 hours at 50°C under argon. Although TLC analysis showed the presence of the three expected dimers, **[Fb-Fb]**, **[Fb-Zn]** and **[Zn-Zn],** and the desired dyad **[Fb-Zn]** could never be obtained pure even after several chromatographic purifications.

Synthesis of dyad* [Fb-Zn], *Procedure B. A solution of **[Fb]** (25 mg, 0.025 mmol), **[Zn]** (27 mg, 0.025 mmol), and palladium(II) acetate (6 mg, 0.026 mmol) in toluene was heated under argon at 80°C for 16 h. TLC monitoring of the advancement showed that the reaction was almost complete. After evaporation of the solvent, the dyad was isolated by column chromatography on silica gel together with the two known homodimers (eluent: cyclohexane/dichloromethane). Crystallization from CH_2Cl_2/CH_3OH afforded the palladium complex **[Fb-Zn]** in about 30% yield (16 mg, 0.0075 mmol). **^1H NMR (400 MHz, 25°C, $CDCl_3$):** δ 9.38 (d, J = 4.8 Hz, 1H, H_{pyrr}), 9.36 (d, J = 4.8 Hz, 1H, H_{pyrr}), 8.90 (d, J = 7.6 Hz, 1H, H_{cyclPh}) 8.88 (d, 1H, J = 7.6 Hz, H_{cyclPh}) 8.72 (d, J = 4.8 Hz, 1H, H_{pyrr}), 8.70 (d, J = 4.8 Hz, 1H, H_{pyrr}), 8.61 (2d, J = 7.6 Hz, 2H,

H_{cyclPh}), 8.57 (d, J = 4.8 Hz, 1H, H_{pyrr}), 8.51 (d, J = 4.8 Hz, 1H, H_{pyrr}), 8.49 (d, J = 4.8 Hz, 1H, H_{pyrr}), 8.45 (d, J = 4.8 Hz, 1H, H_{pyrr}), 8.42 (d, J = 4.8 Hz, 1H, H_{pyrr}), 8.41 (d, J = 4.8 Hz, 1H, H_{pyrr}), 8.30 (s, 1H, H_{N-H}), 8.27 (t, J = 1.6 Hz, 1H, $H_{Ar-para}$), 8.26 (t, J = 1.6 Hz, 1H, $H_{Ar-para}$), 8.21 (s, 1H, H_{N-H}), 8.11 (d, J = 4.8 Hz, 1H, H_{pyrr}), 8.06 (d, J = 1.6 Hz, 1H, $H_{Ar-ortho}$), 8.05 (d, J = 1.6 Hz, 1H, $H_{Ar-ortho}$), 8.02 (d, J = 1.6 Hz, 1H, $H_{Ar-ortho}$), 7.99 (d, J = 1.6 Hz, 1H, $H_{Ar-ortho}$), 7.95 (d, J = 1.6 Hz, 1H, $H_{Ar-ortho}$),7.93 (d, J = 1.6 Hz, 1H, $H_{Ar-ortho}$), 8.1-7.9 (m, 4H, H_{cyclPh}) 7.78 (t, J = 1.6 Hz, 1H, $H_{Ar-para}$), 7.77 (t, J = 1.6 Hz, 1H, $H_{Ar-para}$), 7.73 (t, J = 1.6 Hz, 1H, $H_{Ar-para}$), 7.72 (t, J = 1.6 Hz, 1H, $H_{Ar-para}$), 1.59 (s, 36H, $H_{t\text{Bu}}$), 1.53 (s, 36H, $H_{t\text{Bu}}$), 1.48 (s, 18H, $H_{t\text{Bu}}$), 1.47 (s, 18H, $H_{t\text{Bu}}$), -0.3 (broad, 2H, H_{NH}) ppm. **UV-visible (CH_2Cl_2):** λ_{max} (ε): 374 (59600), 428 (85400), 478 (sh, 102200), 504 (160000), 586 (17900), 634 (24200), 672 (sh, 25300), 691 (34500), 727 nm (19300 $L.mol^{-1}.cm^{-1}$). **ESI MS:** calculated for $C_{138}H_{150}N_{10}O_2PdZn^+$: 2149.03, found: 2149.034. Calculated for $C_{138}H_{152}N_{10}O_2PdZn^{2+}$ ($M+2H^+/2$): 2151.04/2, found: 1075.02.

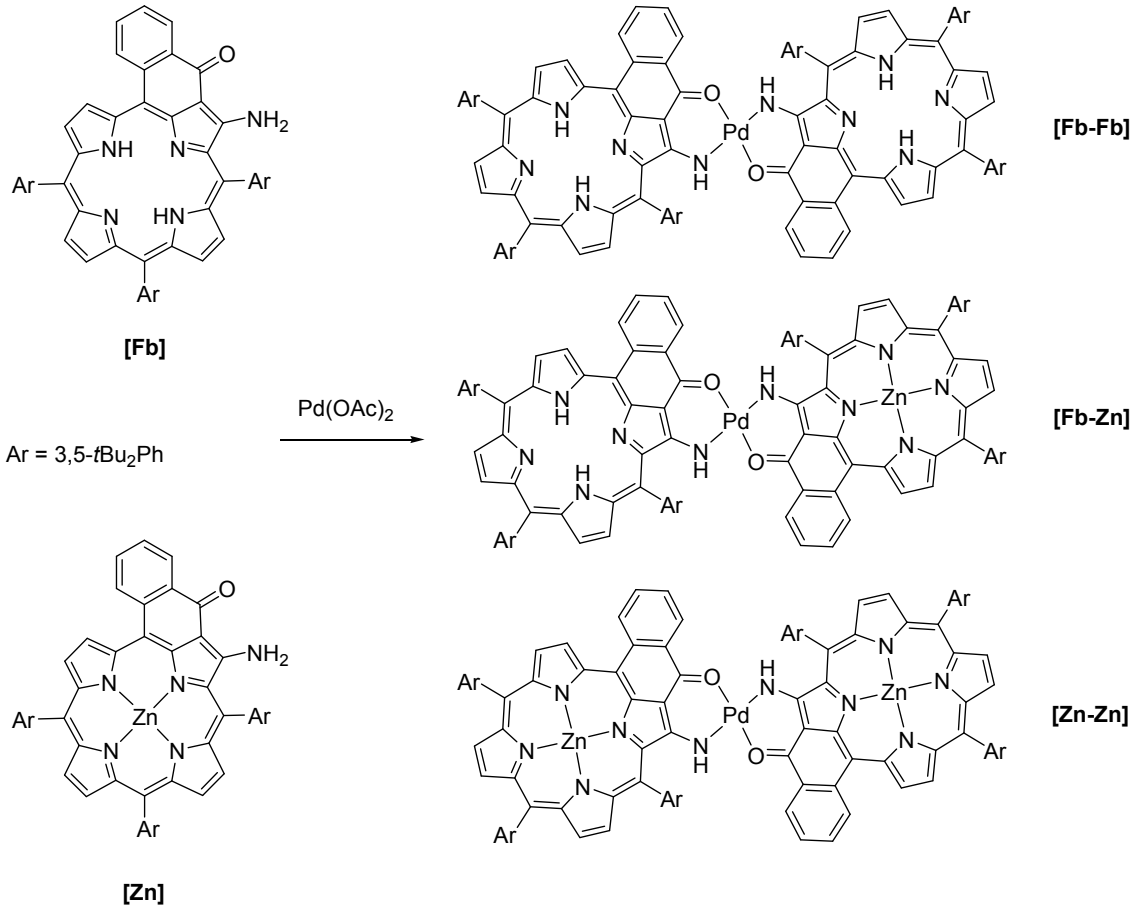

Scheme 1. Synthesis of dyads **[Zn-Zn]**, **[Fb-Zn]** and **[Fb-Fb]**.

Fluorescence quantum yield and lifetimes. The measurements of the emission quantum yields were performed in 2-MeTHF at 298K. Three different measurements (*i.e.* different solutions) were prepared for each photophysical datum (quantum yields and lifetimes). For 298 K measurements samples were prepared under inert atmosphere (in a glove box, $P_{O2} < 25$ ppm). The sample and the standard concentrations were adjusted to obtain an absorbance of 0.05 or less. This absorbance was adjusted to be the same as much as possible for the standard and the sample for a measurement. Each absorbance value was measured five times for better accuracy in the measurements of the quantum yields. The equation $\Phi_s = \Phi_r(F_r/F_s)(I_s/I_r)(n_s/n_r)^2$ was used to calculate the relative quantum yield of each of the sample, where Φ_r is the absolute quantum yield of the reference, n is the refractive index of the solvent, F is the absorptance ($F= 1\text{-}10^{-A}$, where A is the absorbance) at the excitation wavelength, and I is the integrated area under the corrected emission curve. The subscripts s and r refer to the sample and reference, respectively. A solution of free base *meso*-tetraphenylporphyrin (H_2TPP) in 2-MeTHF ($\Phi_F = 0.11$)[2] was used as the external reference. The emission lifetimes in the 1 to 10 ns range were measured on a TimeMaster model TM-3/2003 apparatus from PTI. The source was a nitrogen laser with high-resolution dye laser (fwhm~1400 ps) and the excited lifetimes were obtained from deconvolution or distribution lifetimes analysis. Time resolved photoluminescence measurement was done by using Titan-sapphir with regenerative amplificator as the laser source and Axis Photonique Inc. AXIS-TRS Streak camera was used as a detector. This detector allowed measurement in the time window of 3 ps to ~3 ns (see below). The data analyses were made using open source software named Glotaran 1.3. This technique allows for the reliable measurements of fluorescence lifetime between 8 ps and 2 ns. Any lifetime above this value is not accurate.

Femptosecond transient absorption spectroscopy. The fs transient spectra and decay profiles were acquired on an homemade system using the SHG of a Soltice (Spectra Physics) Ti-Sapphire laser (λ_{exc} = 398 nm; FWHM = 75 ps; pulse energy = 0.1 μJ/pulse, rep. rate = 1 kHz; spot size ~ 500 μm), a white light continuum generated inside a Sapphire window and a custom made dual CCD camera of 64 x 1024 pixels sensitive between 200 and 1100 nm (S7030, Spectronic Devices). The delay line permitted to probe up to 4 ns with an accuracy of ~4 fs. The results were analysed with the program Glotaran (*http://glotaran.org*) permitting to extract a sum of

independent exponentials ($I(\lambda,t) = C_1(\lambda)\bullet\exp(-t/\lambda_1)+C_2(\lambda)\bullet \exp(-t/\lambda_2)+\ldots$) that fits the whole 3D transient map.

Fast kinetic fluorescence measurements: The search for short components (3 ps < τ_F <~3 ns) of the fluorescence decays were performed using the output of an OPA (OPA-800CF, Spectra-Physics) operating at λ_{exc} = 635 nm, pulse width of 90 ps, rep. rate = 1 kHz, pulse energy = 1.6 μJ/pulse, spot size ~2 mm, and a Streak Camera (Axis-TRS, Axis Photonique Inc.) with less than 3 and 8 ps time resolution respectively at 298 and 77K. The results were also globally analysed with the program Glotaran (*http://glotaran.org*) permitting to extract a sum of independent exponentials ($I(\lambda,t) = C_1(\lambda)\bullet \exp(-t/\tau_1)+C_2(\lambda)\bullet\exp(-t/\tau_2)+\ldots$).

Computational Methodology. Computational Methodology. All density functional theory (DFT) calculations were performed with Gaussian 09[3] at the Université de Sherbrooke with the MP2 supercomputer supported by Le Réseau Québécois De Calculs Hautes Performances. The DFT [4-7] geometry optimisations as well as TD-DFT calculations [8-10] were carried out using the B3LYP method.[11-13] 6-31g* basis sets [14-20] were used for the porphyrin macrocycles. 3-21g*[21-26] basis sets were used for the phenyl groups of the porphyrin and tert-butyl groups attached to the phenyl. VDZ (valence double ζ) with SBKJC effective core potentials [27-29] were used for Zn, Pd. The calculated absorption spectra, were obtained from GaussSum 2.1.[30] No solvent field was applied. It was not necessary for the purpose of this work.

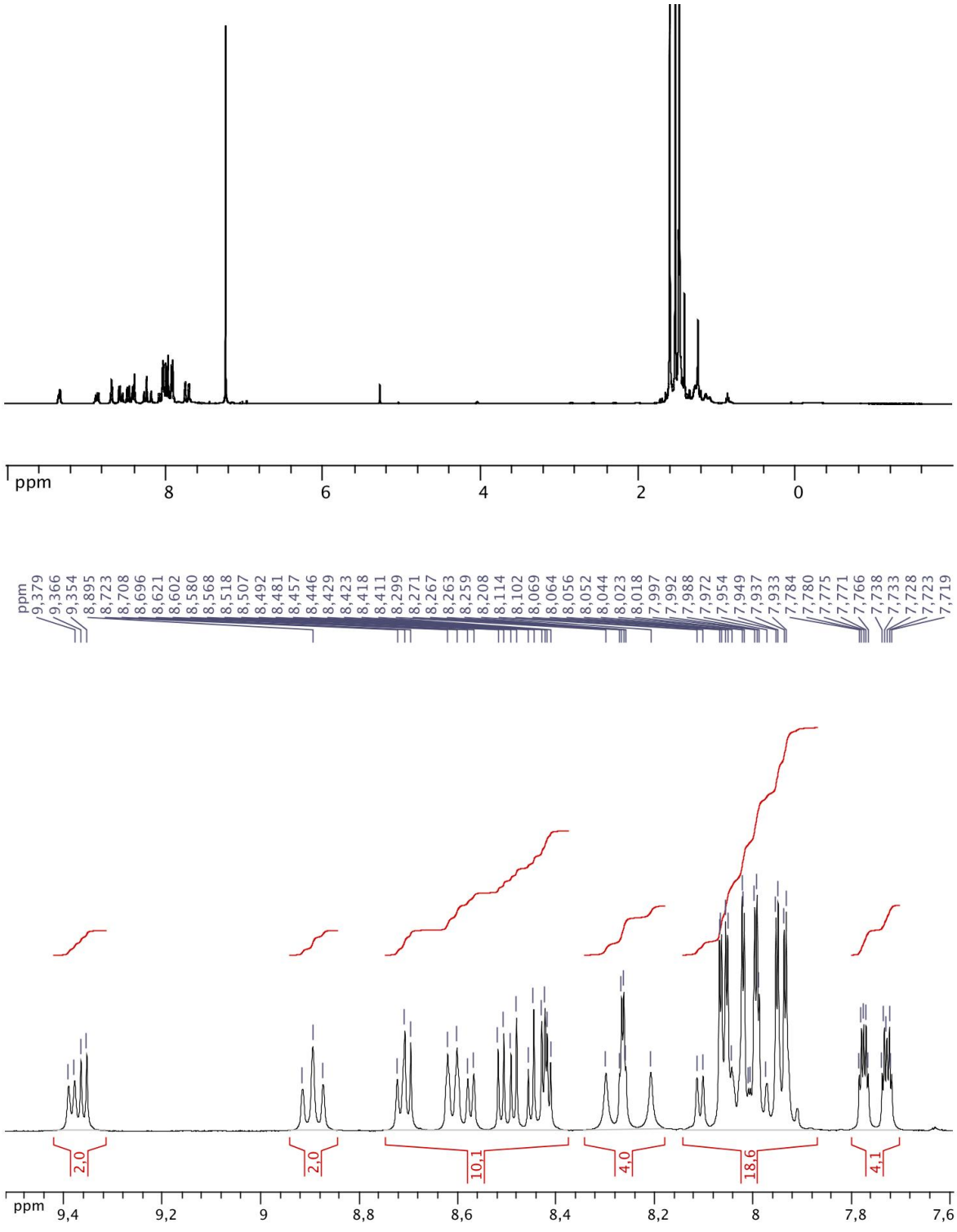

Figure S1. ^{1}H NMR of **[Fb-Zn]** in $CDCl_3$ (bottom: expansion of the aromatic region).

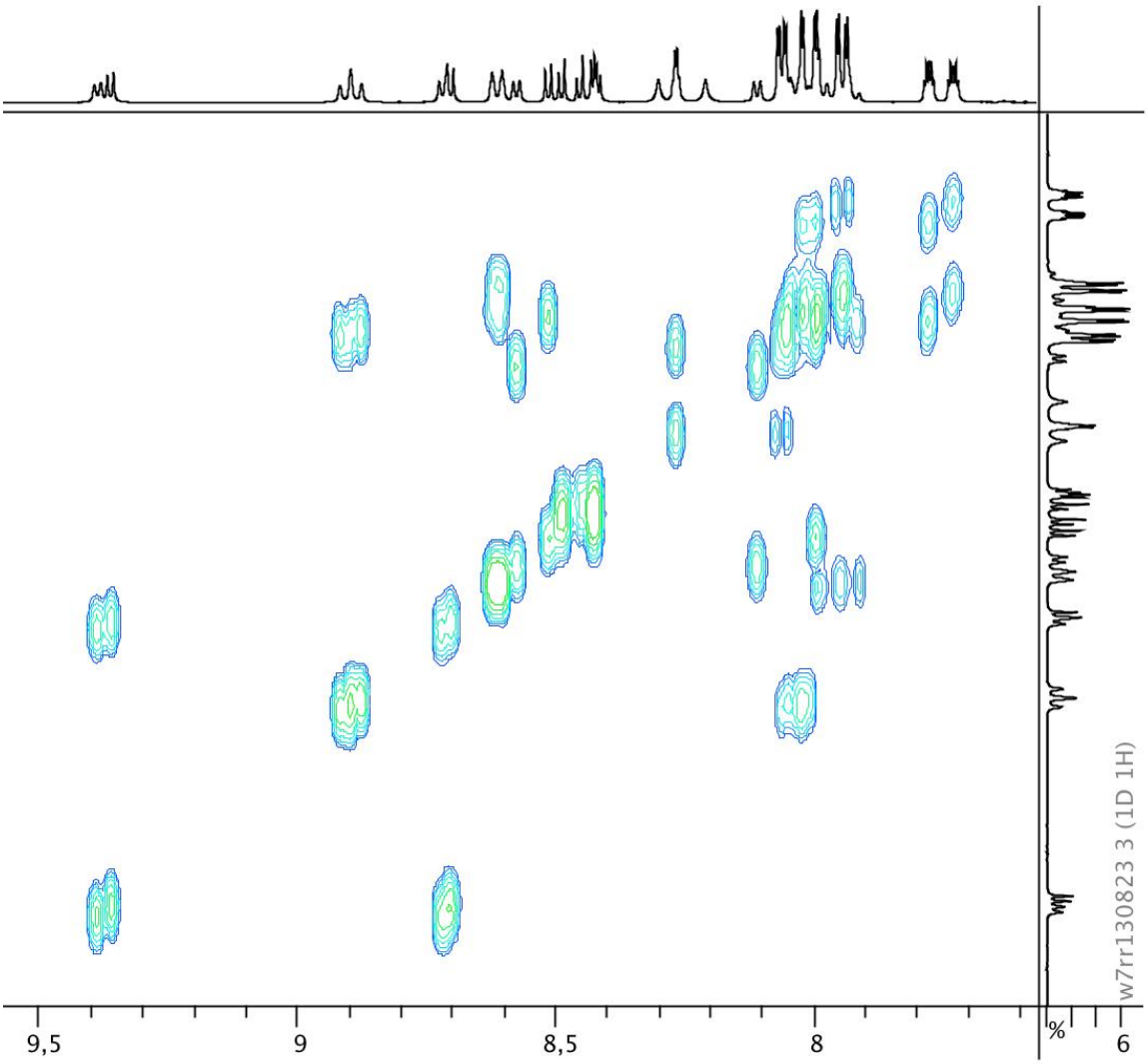

Figure S2. ^{1}H-^{1}H COSY spectrum of **[Fb-Zn]** in $CDCl_3$ (aromatic region only).

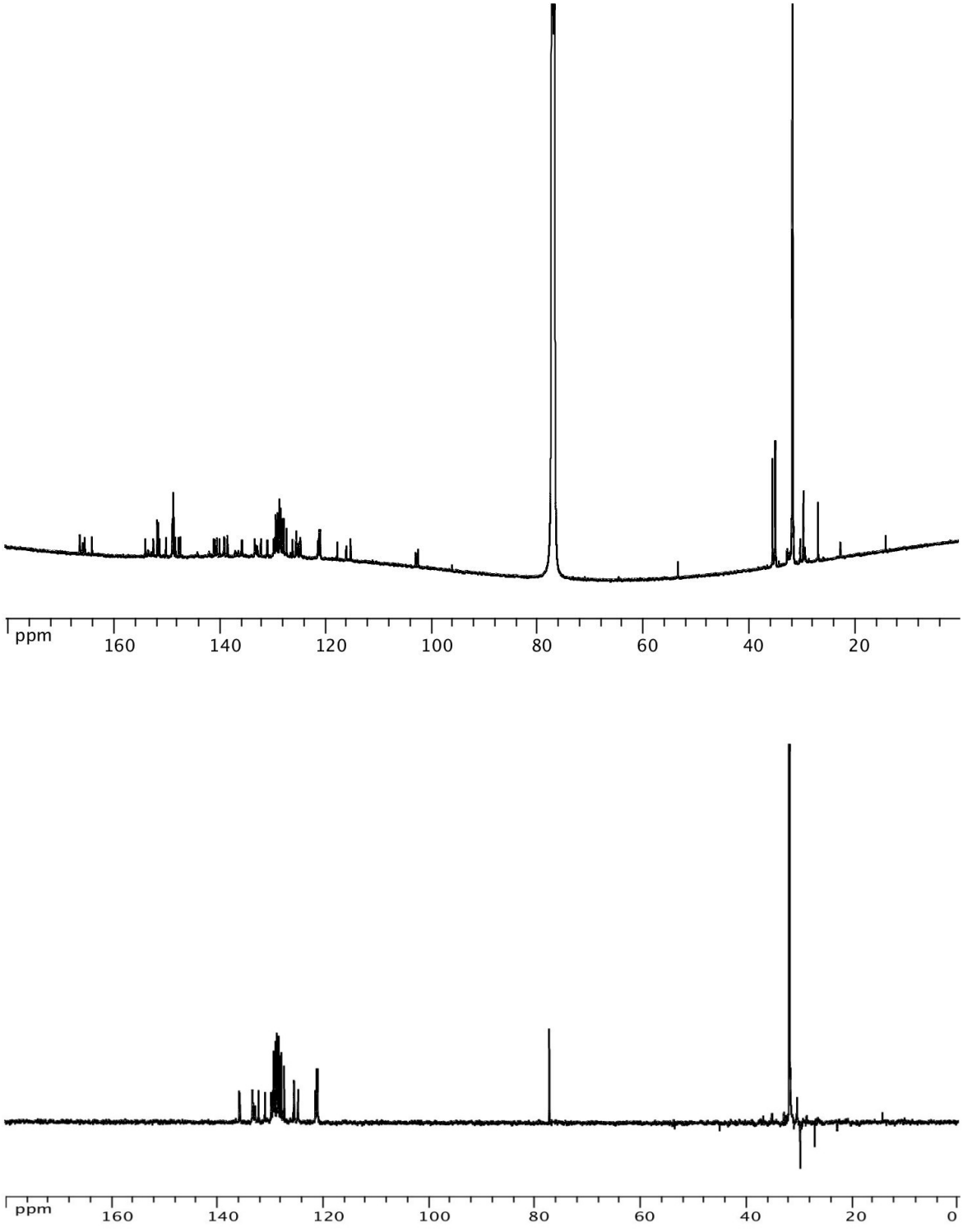

Figure S3. ^{13}C (top) and DEPT135 (bottom) of **[Fb-Zn]** in $CDCl_3$ (cryo, 125 MHz).

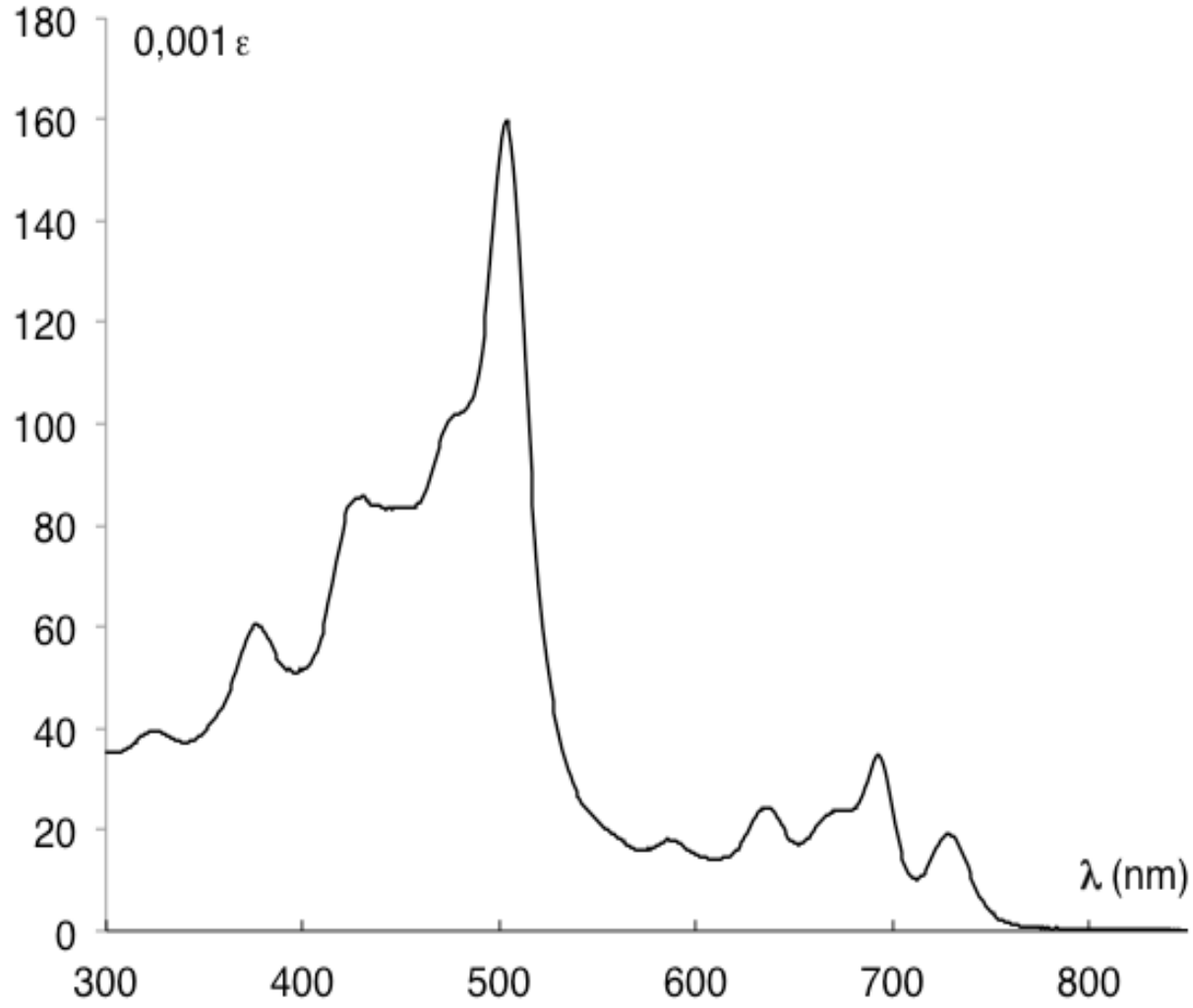

Figure S4. Absorption spectrum of **[Fb-Zn]** in CH_2Cl_2.

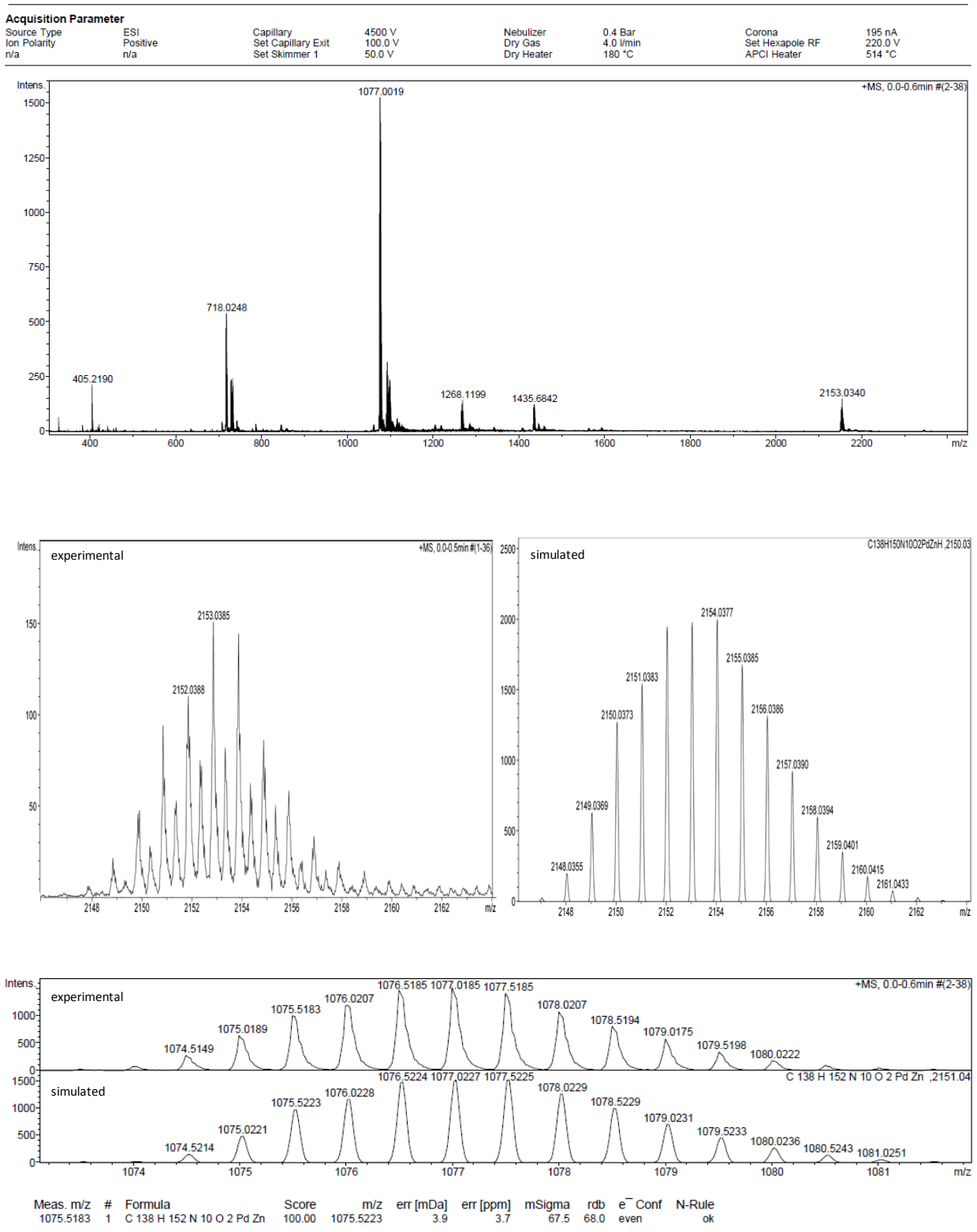

Figure S5. Experimental and simulated mass spectra (ESI mass) of **[Fb-Zn]**.

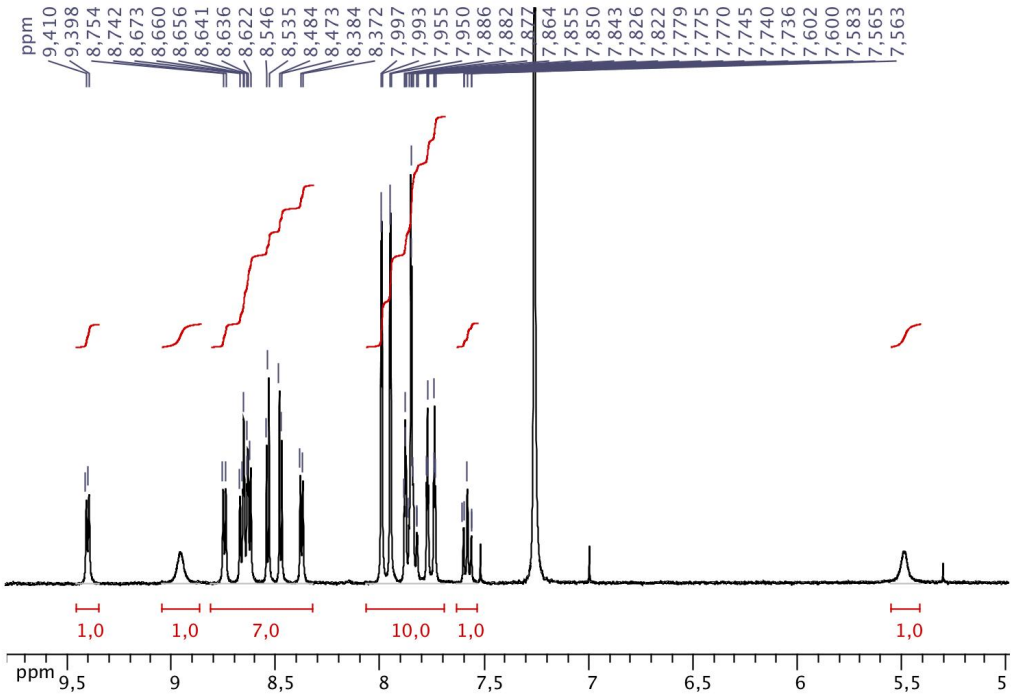

Figure S6. ^{1}H NMR of **[Fb]** in $CDCl_3$ (aromatic part).

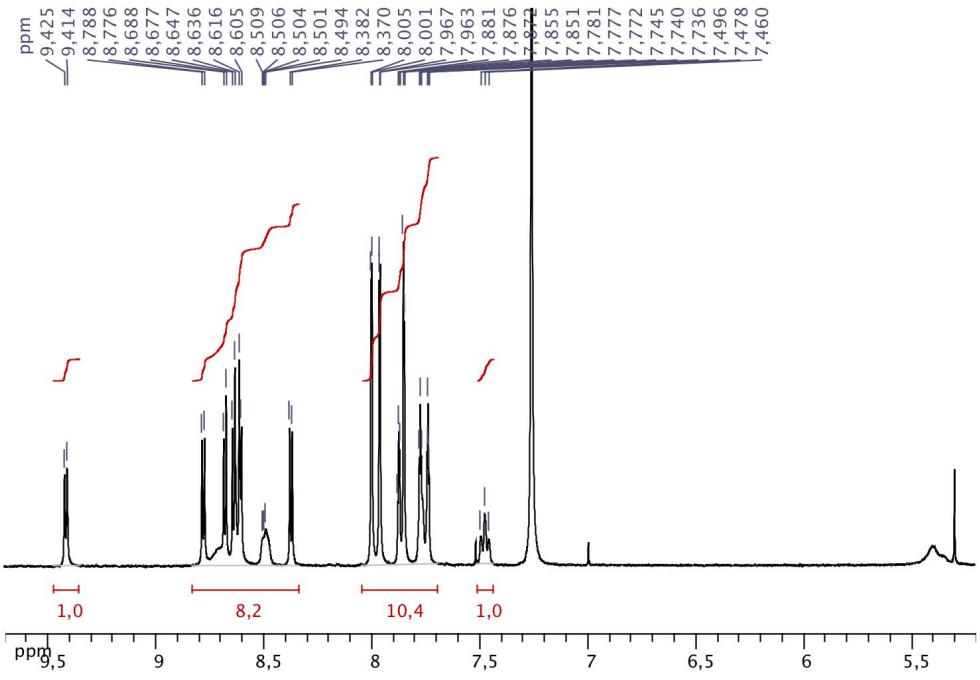

Figure S7. ^{1}H NMR of **[Zn]** in $CDCl_3$ (aromatic part).

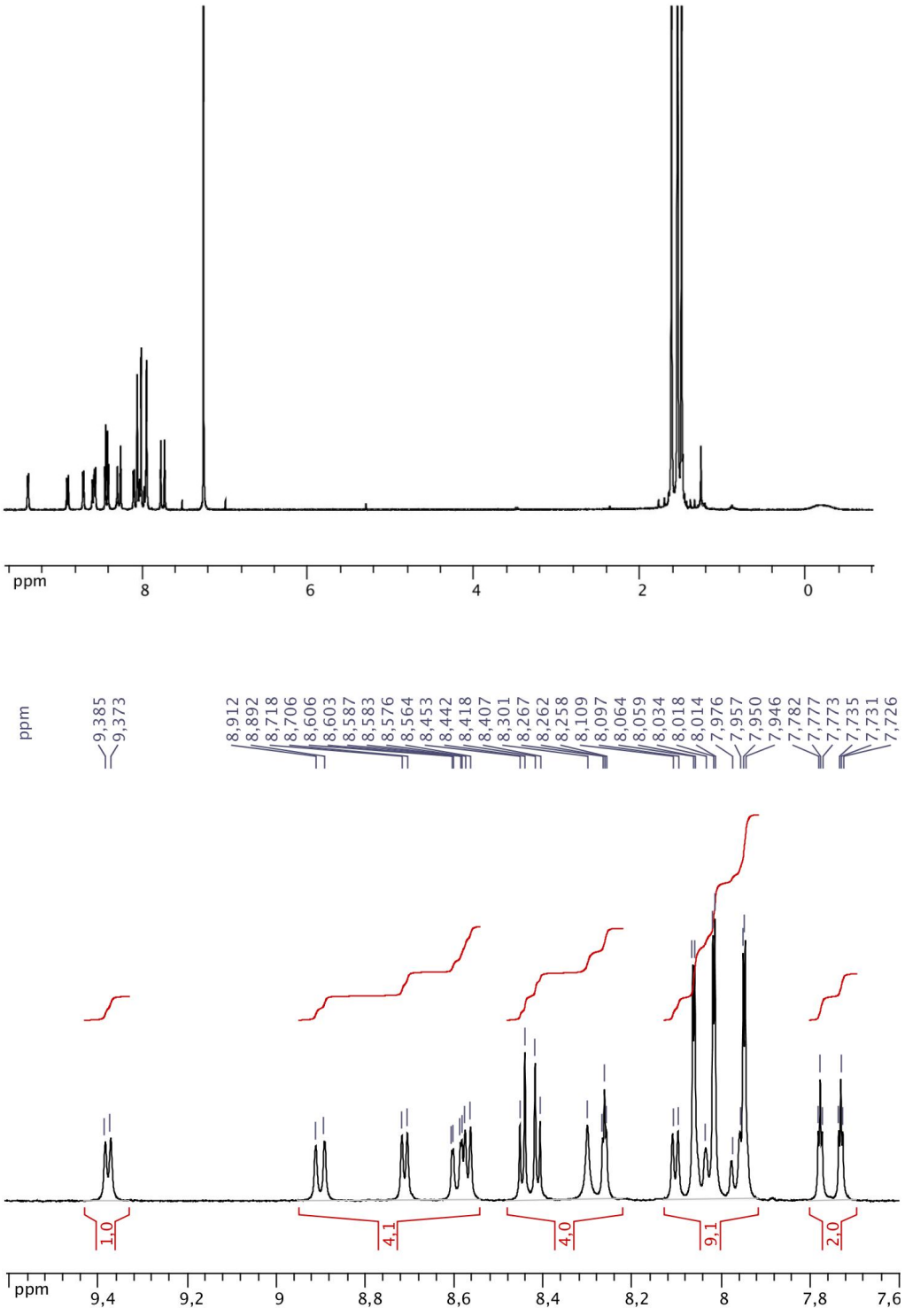

Figure S8. ^{1}H NMR of **[Fb-Fb]** in $CDCl_3$ (bottom: expansion of the aromatic region).

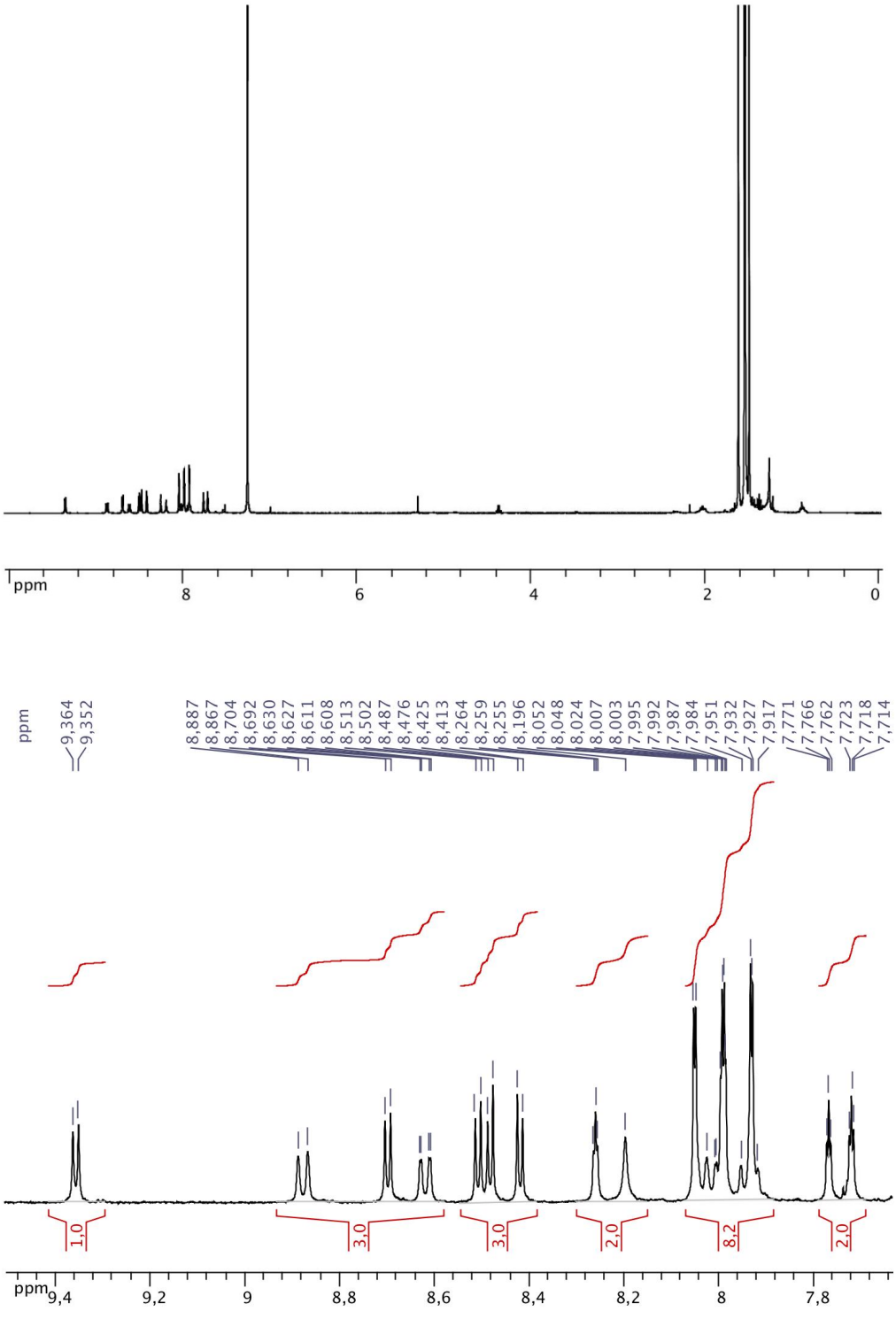

Figure S9. ^{1}H NMR of **[Zn-Zn]** in $CDCl_3$ (bottom: expansion of the aromatic region).

Table S1. Absorption data.

Compound	**λ_{max} (nm), ε ($M^{-1}.cm^{-1}$) in CH_2Cl_2 at 298 K**	**λ_{max} (nm) at 77 K in 2-MeTHF**
[Zn]	382 (42100), 466 (170900), 608 (13300), 664 (31900).	388, 476, 562, 624, 664.
[Fb]	315 (28200), 371 (46200), 394 (47300), 456 (107800), 571 (9100), 617 (21500), 711 (8500).	372, 396, 450, 568, 616, 706.
[Zn-Zn]	378 (75800), 428 (100800), 500 (246000), 634 (31100), 674 (53700), 696 (75400).	380, 428, 508, 592, 636, 698.
[Fb-Fb]	375 (85000), 429 (119000), 475 (11900), 507 (182000), 588 (31500), 639 (34300), 660 (25300), 730 (39000).	378, 426, 478, 508, 588, 638, 728.
[Fb-Zn]	374 (59600), 428 (85400), 503 (160000), 586 (17900), 634 (24200), 691 (34500), 727 (19300).	378, 446, 484, 512, 592, 638, 694, 728.

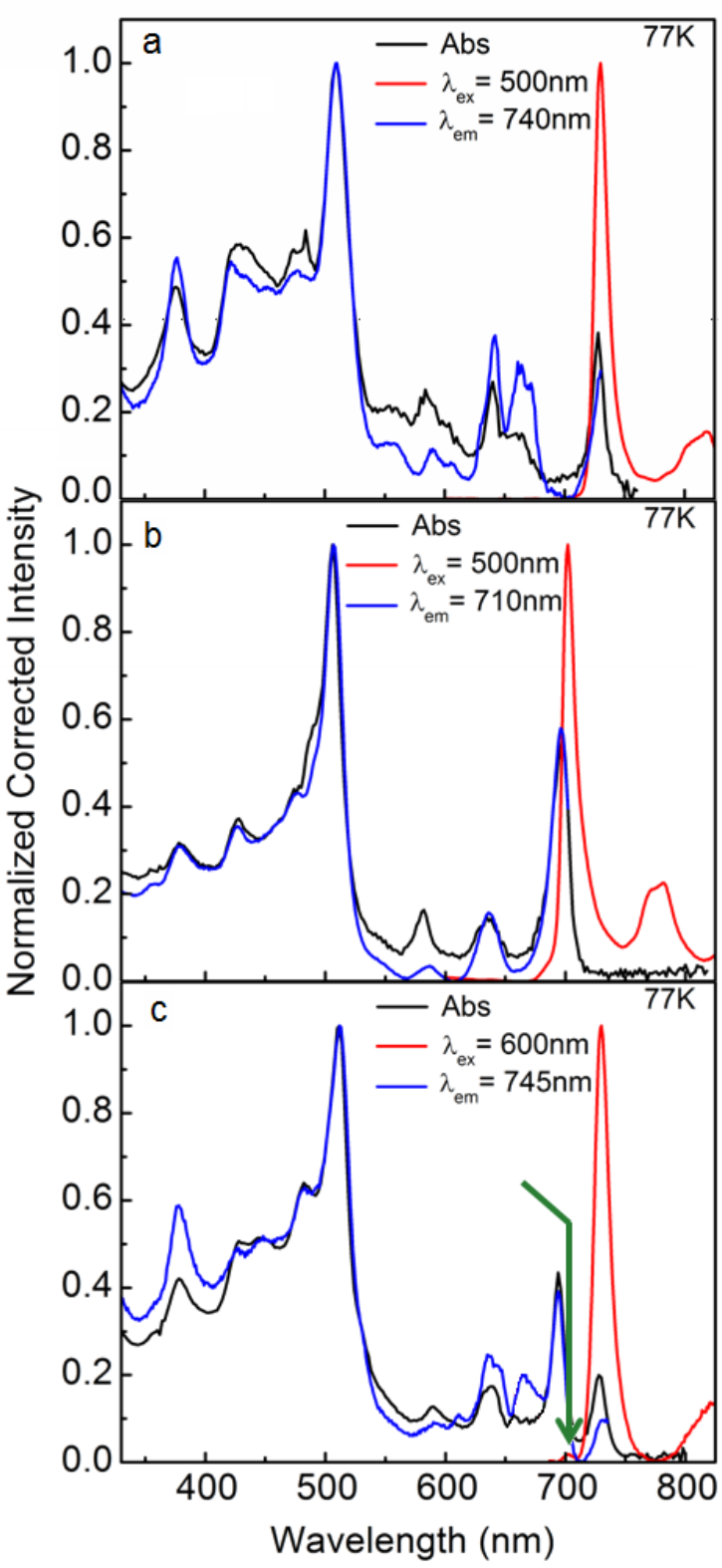

Figure S10. Absorption (black), fluorescence (red) and excitation (blue) spectra of **[Fb-Fb]** (**a**), **[Zn-Zn]** (**b**), and **[Fb-Zn]** (**c**) in 2-MeTHF at 77 K. The green arrow stresses the weak donor fluorescence.

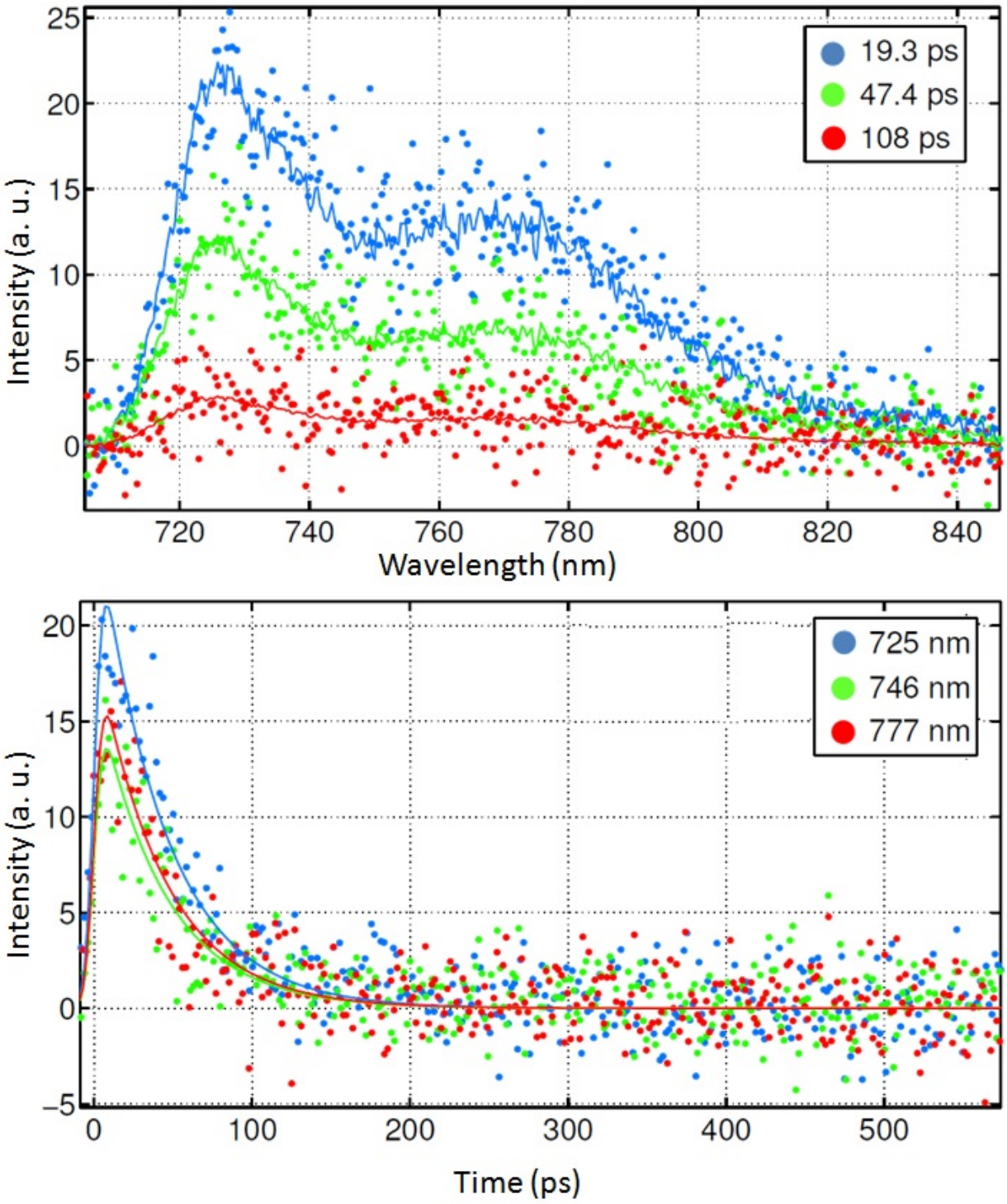

Figure S11. Time resolved fluorescence spectra of **[Zn-Zn]** in 2-MeTHF at 298 K using the Streak camera. Top: time-resolved spectra. Bottom: decay traces. The best fits are all monoexponential.

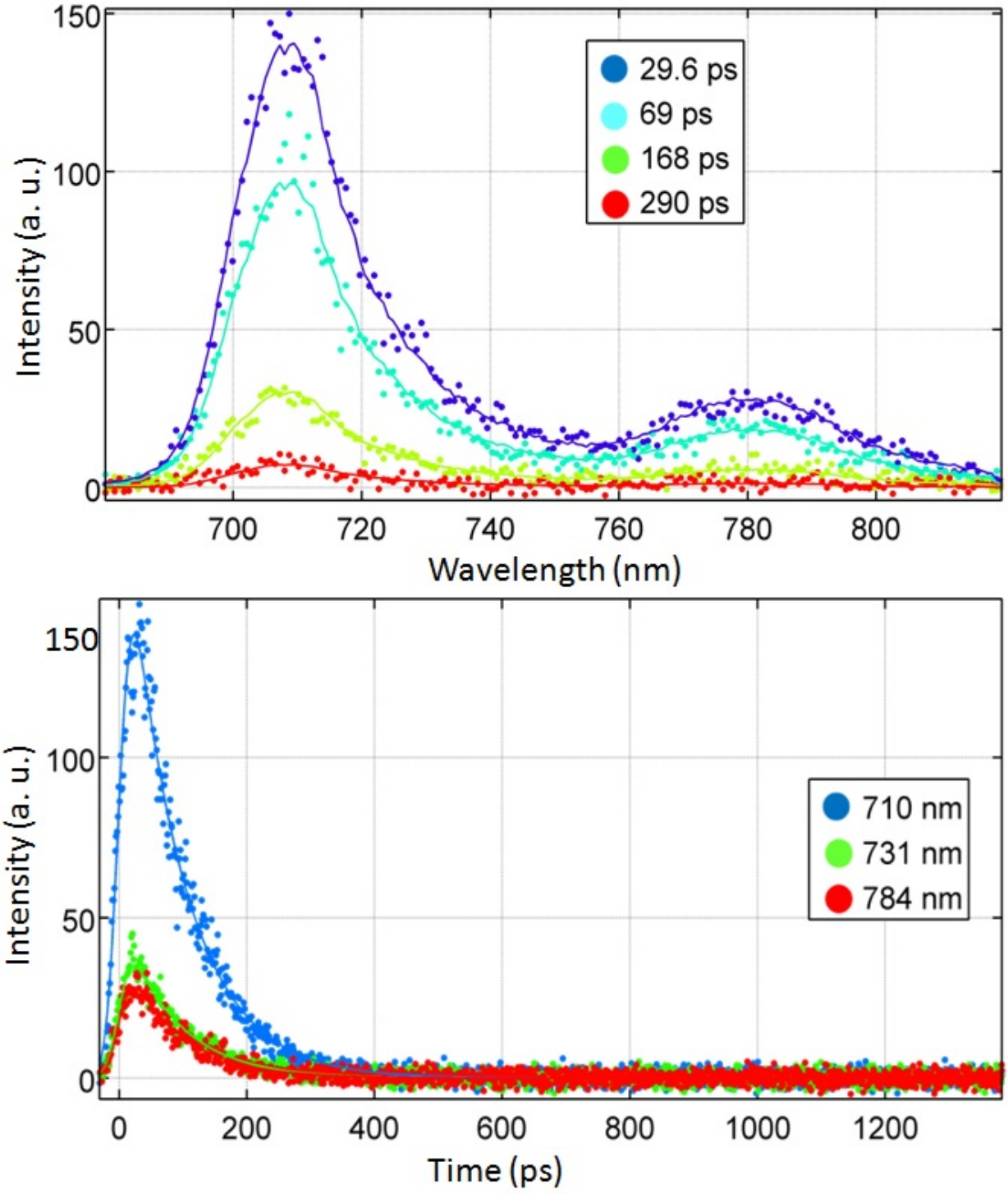

Figure S12. Time resolved fluorescence spectra of **[Zn-Zn]** in 2-MeTHF at 77 K using the Streak camera. Top: time-resolved spectra. Bottom: decay traces. The best fits are all monoexponential.

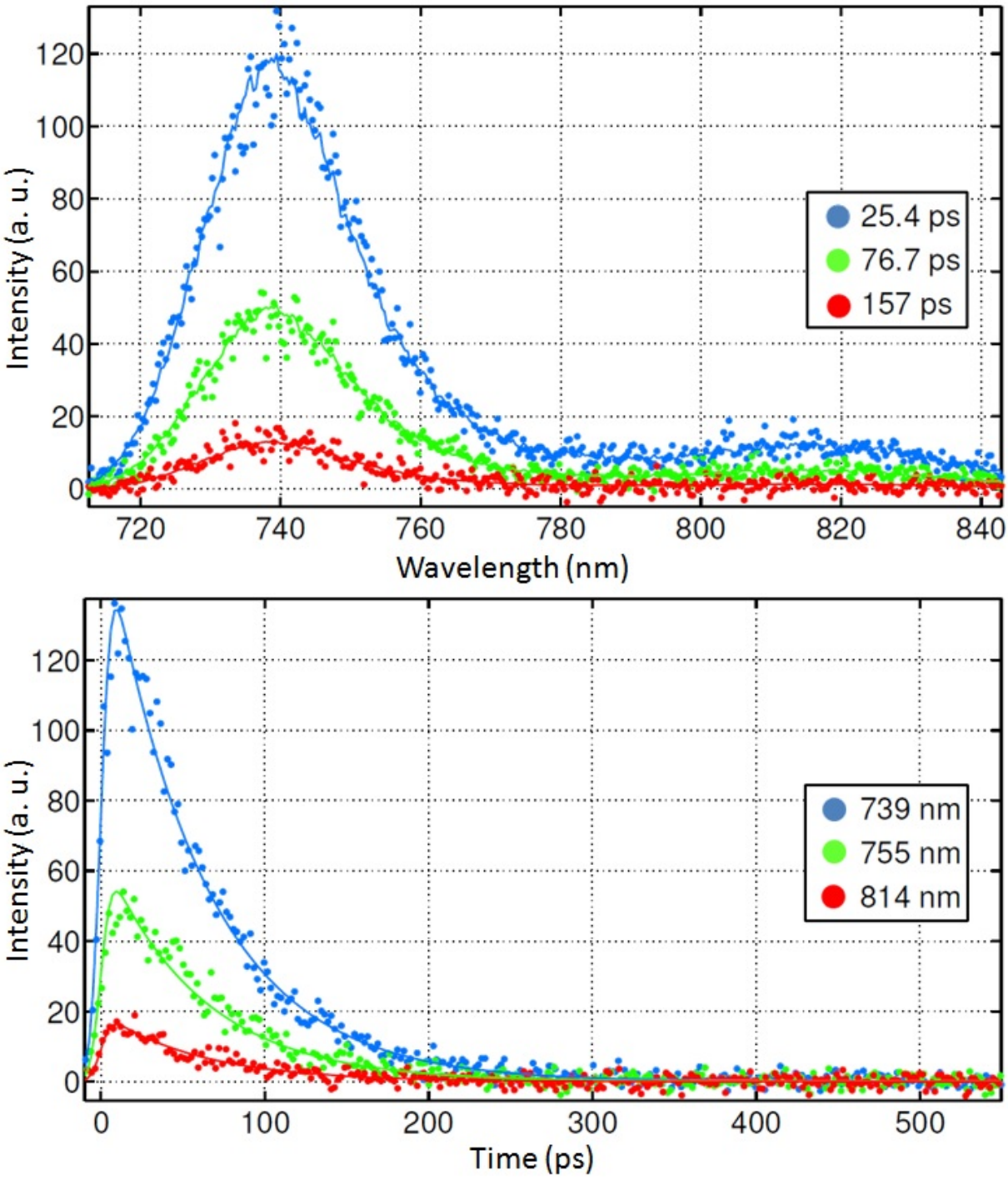

Figure S13. Time resolved fluorescence spectra of **[Fb-Fb]** in 2-MeTHF at 298 K using the Streak camera. Top: time-resolved spectra. Bottom: decay and rise traces.

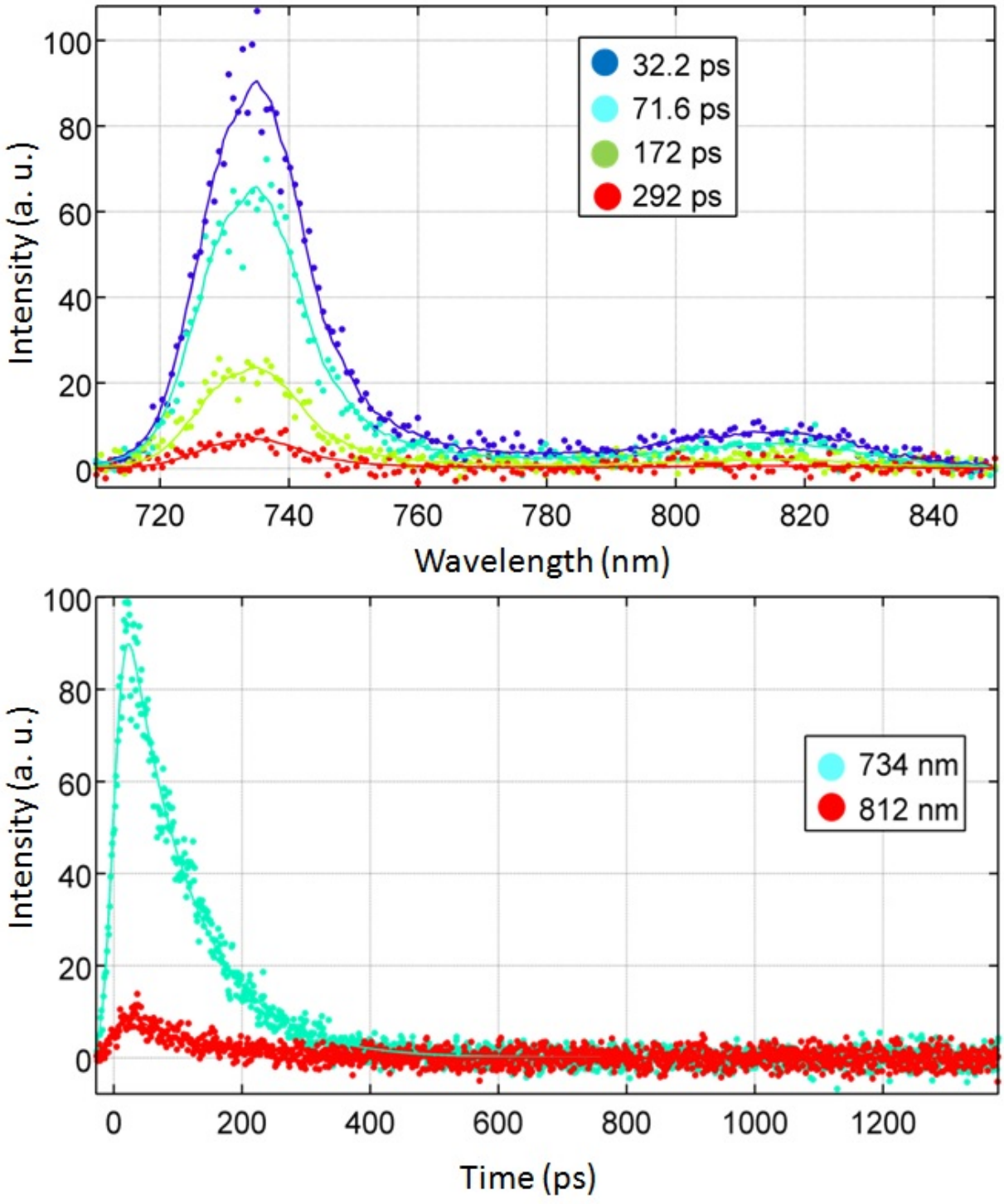

Figure S14. Time resolved fluorescence spectra of **[Fb-Fb]** in 2-MeTHF at 298 K using the Streak camera. Top: time-resolved spectra. Bottom: decay traces. The best fits are all monoexponential.

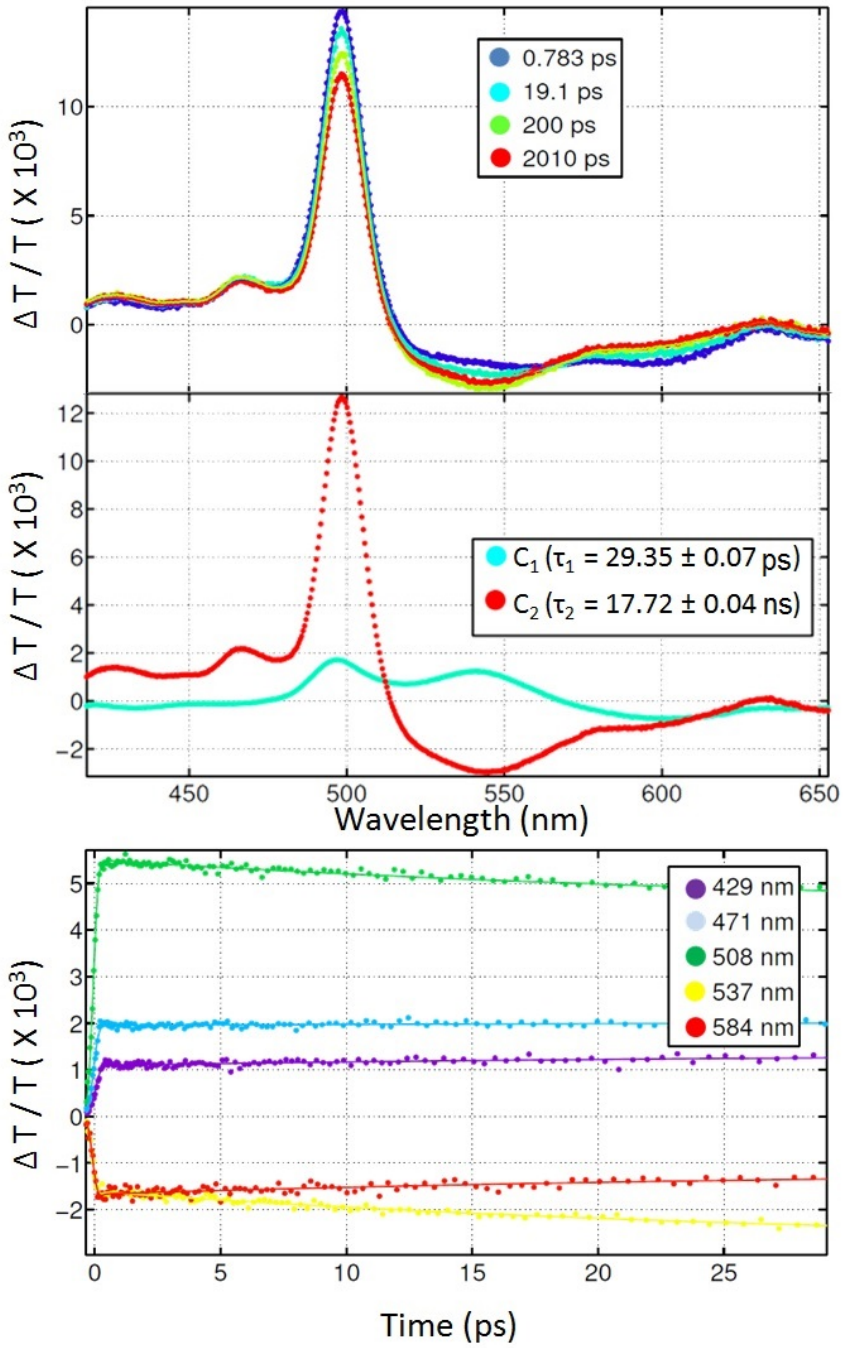

Figure S15. Transient absorption spectra of **[Zn-Zn]** in 2-MeTHF at 298 K (up), reconstruction of the transient spectra of the various intermediates (middle) and decay and rise traces monitored at various wavelengths (bottom). The fast decays and rise traces are due to the direct absorption of the laser light (<<1ps). The values indicated inside the insets (middle frame) are values extracted from the best fits. The value at ~29.4 ps is the S_1 transient (τ_F measured on the Streak camera is 43 ps). The transient at relaxing at 17.7 ns is the triplet state, T_1. This value should not be considered accurate because of the delay line used (3.3 ns).

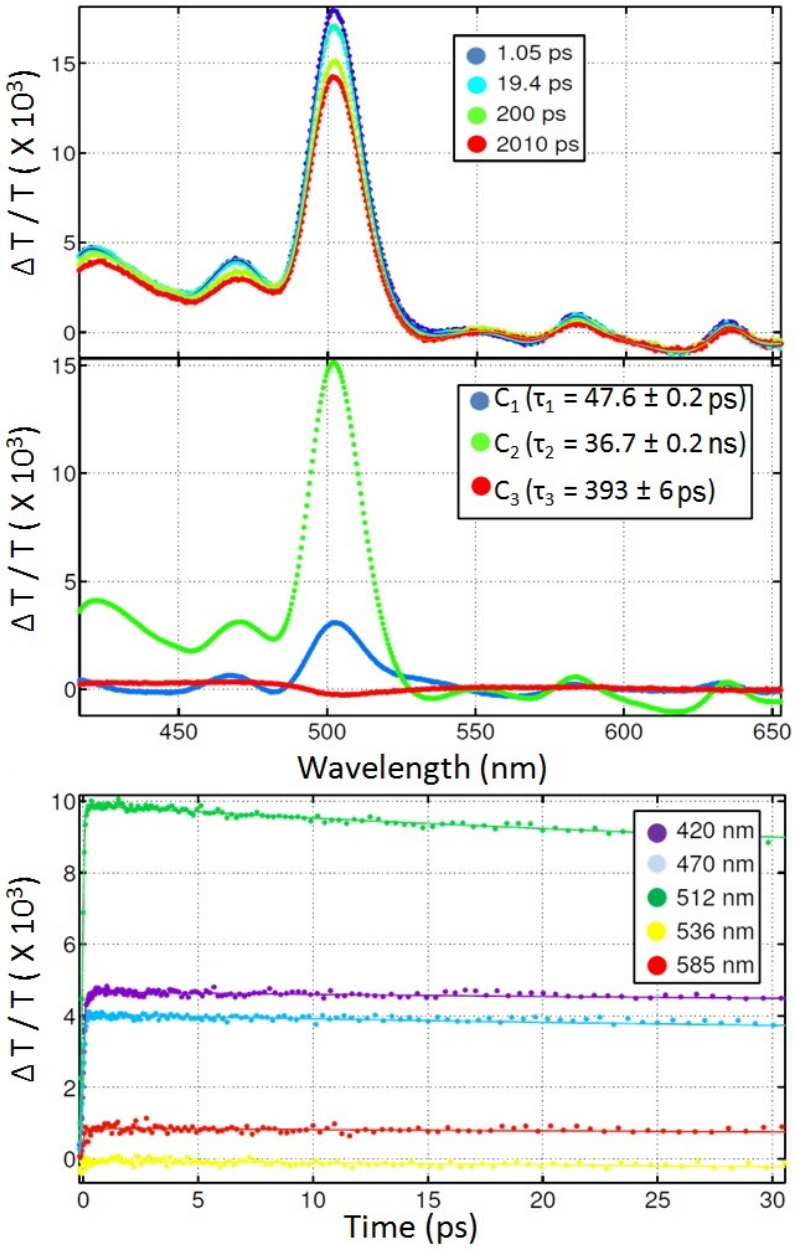

Figure S16. Transient absorption spectra of **[Fb-Fb]** in 2-MeTHF at 298 K (up), reconstruction of the transient spectra of the various intermediates (middle) and decay and rise traces monitored at various wavelengths (bottom). The values indicated inside the insets (middle frame) are values extracted from the best fits. The species relaxing at ~48 ps is associated with the S_1 transient. (τ_F measured on the Streak camera is 59.7 ps). The transient at relaxing at 36.7 ns is the triplet state, T_1. This value should not be considered accurate because of the delay line used (3.3 ns). The component with a relaxation time of 0.39 ns is very weak and may very likely be unreal.

Optimized geometries in the ground state and frontier MO representations (DFT)

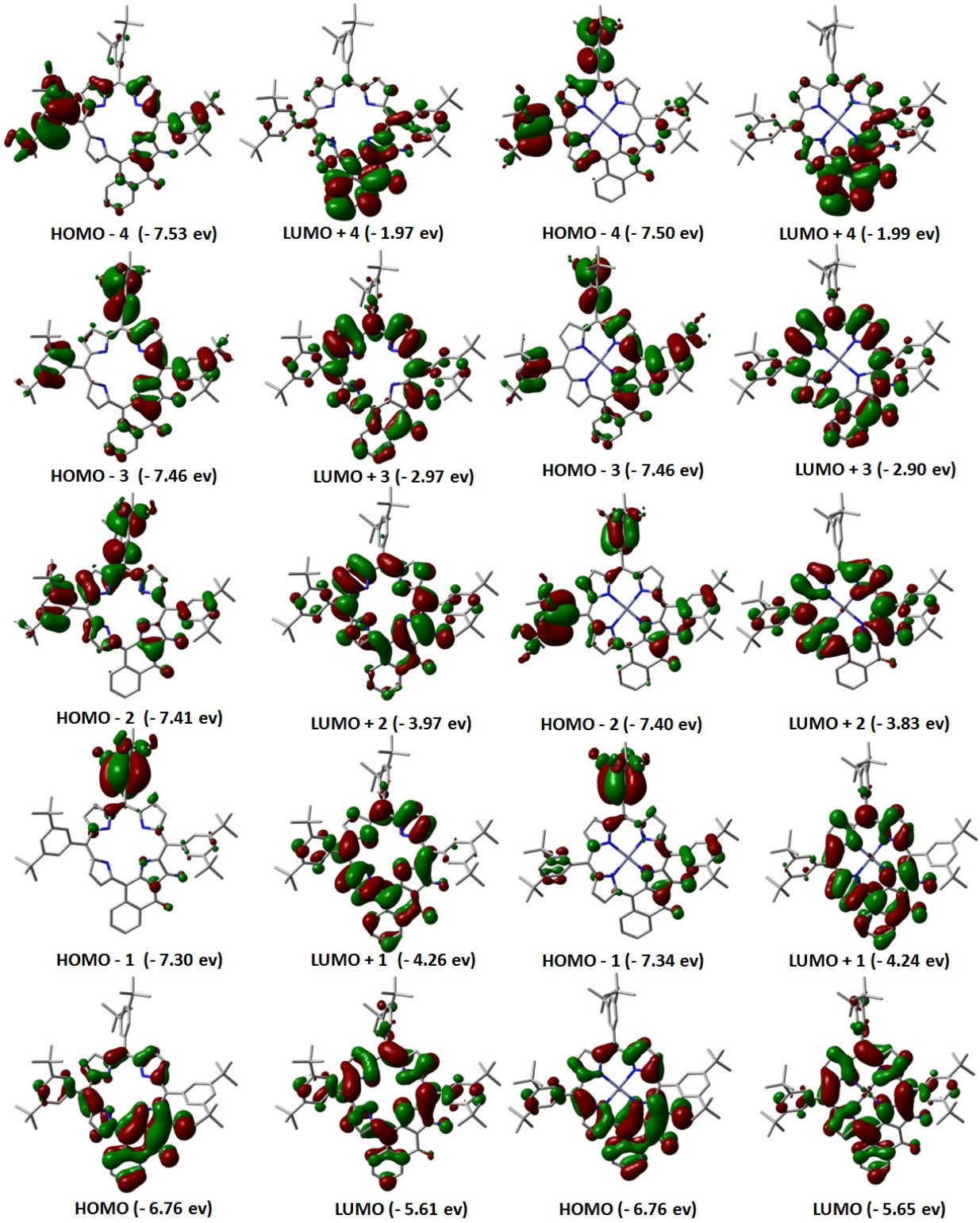

Figure S17. Representation of the frontier MOs for **[Fb]** (left) and **[Zn]** (right).

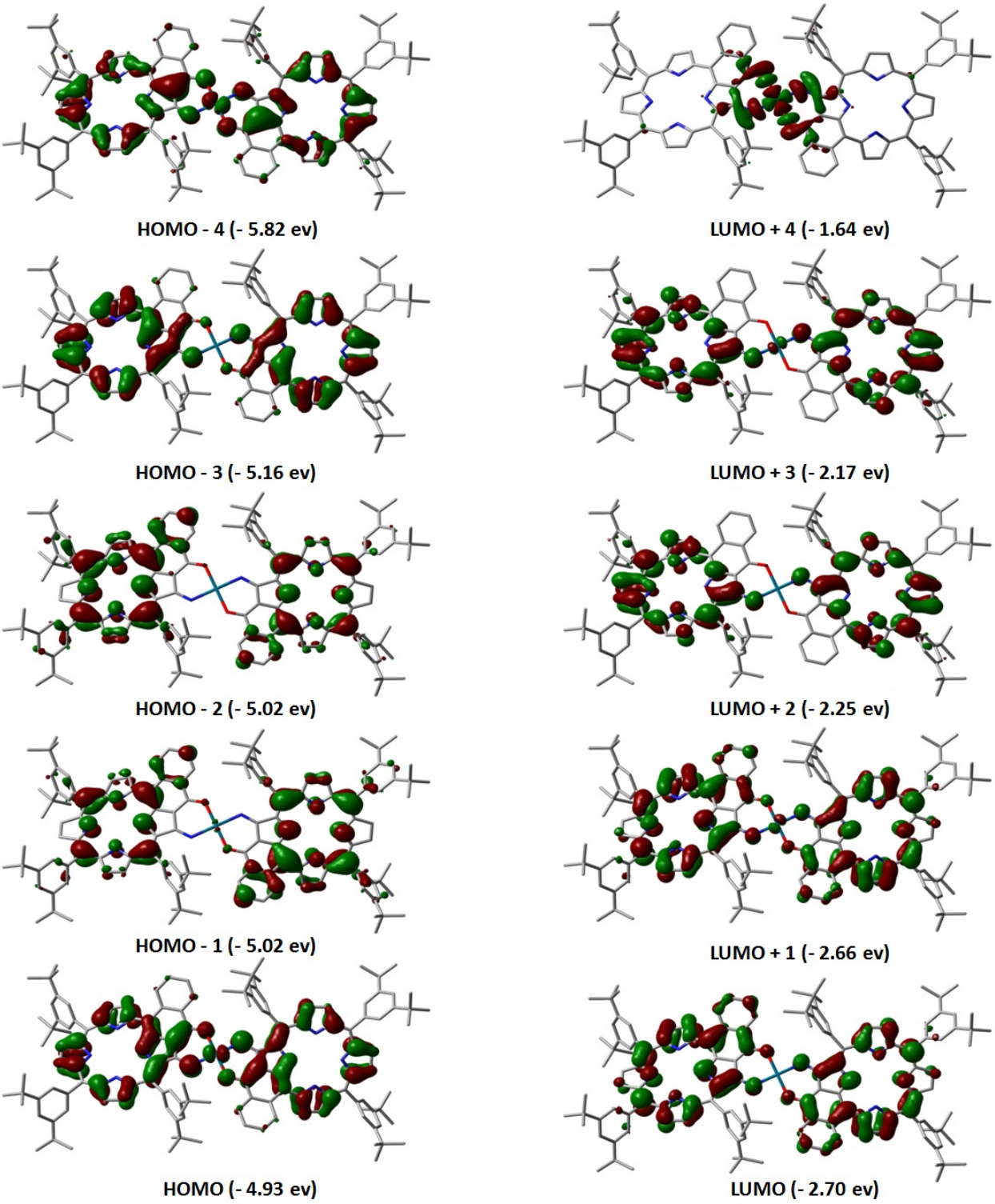

Figure S18. Representation of the frontier MOs for **[Fb-Fb]**.

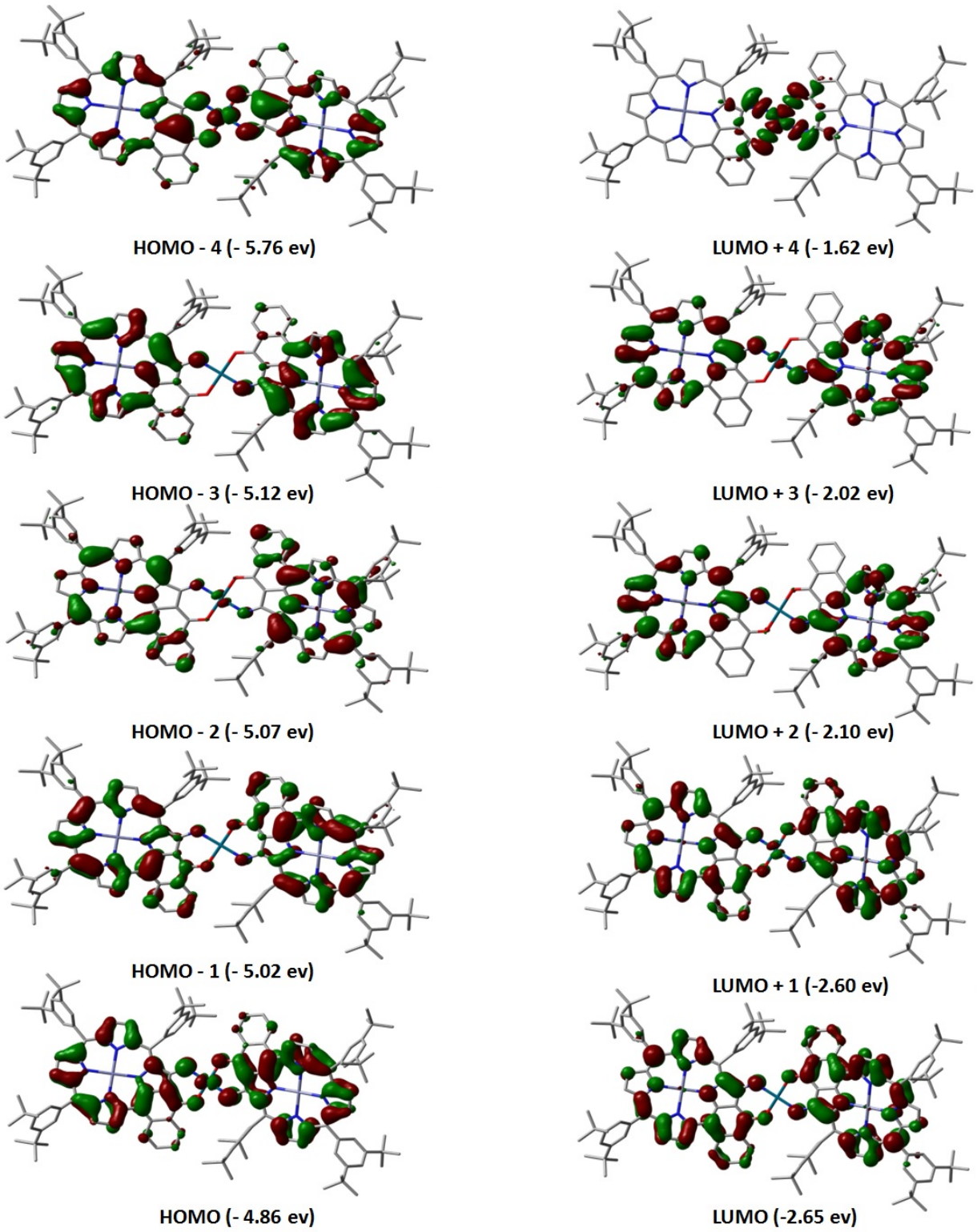

Figure S19. Representation of the frontier MOs for **[Zn-Zn]**.

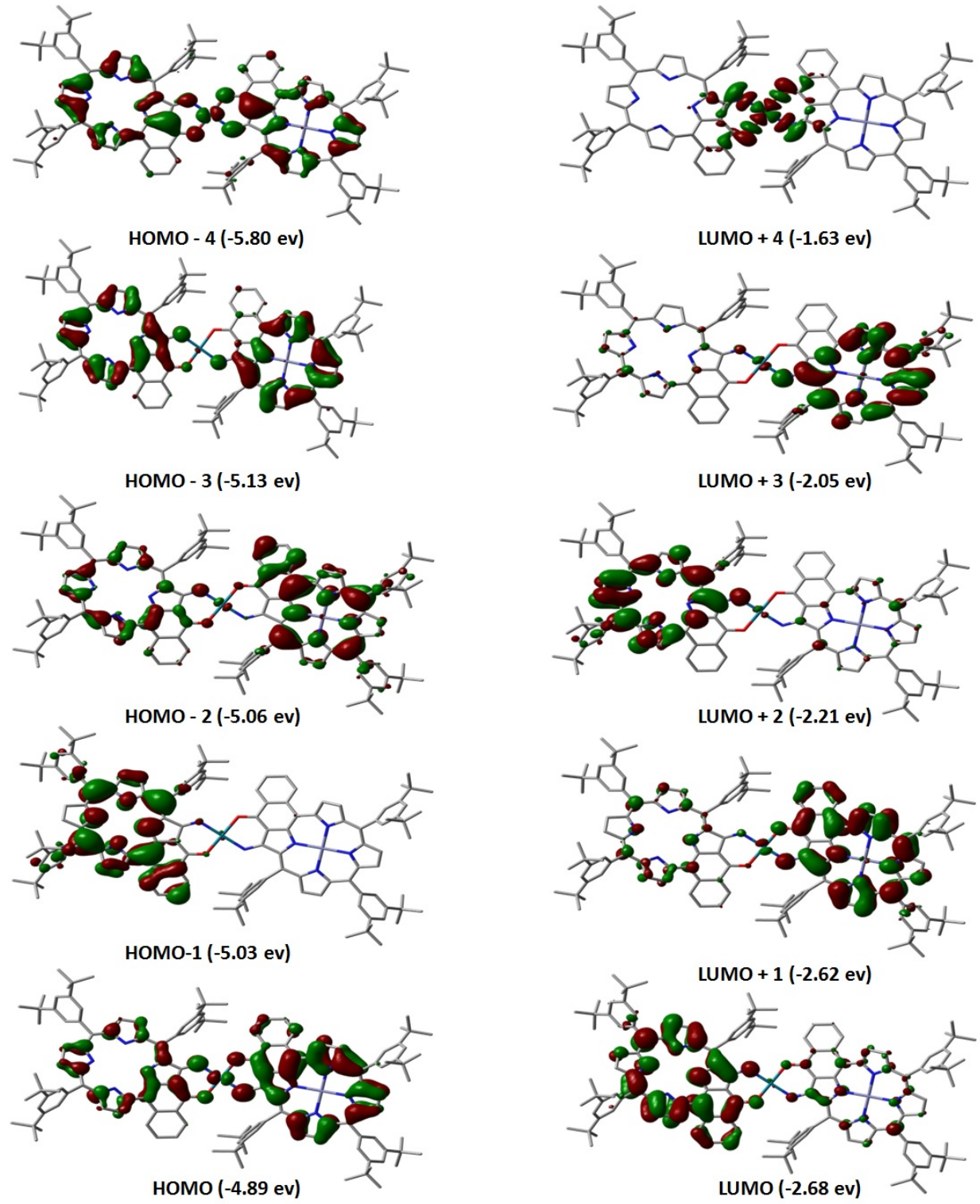

Figure S20. Representation of the frontier MOs for **[Fb-Zn]**, the HOMO+4 and LUMO-4 are new in comparison with Fig. 4 in the text.

Atomic Contributions to the MOs

The tables below show the % electronic contributions over given molecular fragments from HOMO-4 to LUMO+4. H and L refer to the HOMO and LUMO orbitals respectively. The fragments are listed on the left of the table. The fragments exhibiting the largest atomic contributions (*i.e.* > 10%) are highlighted in grey.

Table S2. Relative atomic contributions of the various fragments in **[Fb-Fb]**.[a]

	H-4	H-3	H-2	H-1	HOMO	LUMO	L+1	L+2	L+3	L+4
Pd	7.72	0.43	0.01	0.22	5.42	0.05	1.01	0.37	0.96	39.02
[Fb1]	45.59	49.72	57.71	41.45	47.09	50.47	48.57	50.07	48.88	30.41
[Fb2]	45.79	49.53	41.59	57.56	47.29	49.08	49.92	49.18	49.80	30.41
*t*Bu groups	0.90	0.32	0.69	0.77	0.20	0.40	0.49	0.38	0.36	0.17

a) **[Fb1]** and **[Fb2]** are the free base porphyrin chromophores.

Table S3. Relative atomic contributions of the various fragments in **[Zn-Zn]**.[a]

	H-4	H-3	H-2	H-1	HOMO	LUMO	L+1	L+2	L+3	L+4
Pd	8.90	0.13	1.03	0.24	4.54	0.05	1.25	0.41	0.95	40.72
Zn 1	0.08	0.36	0.54	0.24	0.04	0.12	0.12	0.10	0.10	0.04
Zn 2	0.08	0.34	0.55	0.25	0.04	0.12	0.13	0.10	0.11	0.04
[Zn1]	45.01	50.24	48.15	49.17	47.29	50.56	48.13	50.28	48.45	29.53
[Zn2]	45.14	48.53	49.00	49.46	47.79	48.74	49.90	48.70	50.00	29.53
*t*Bu groups	0.79	0.40	0.73	0.64	0.29	0.41	0.47	0.41	0.39	0.14

a) **[Zn1]** and **[Zn2]** are Zn-containing porphyrin chromophores minus the Zn atom.

Table S4. Relative atomic contributions of the various fragments in **[Fb-Zn]**.[a]

	H-4	H-3	H-2	H-1	HOMO	LUMO	L+1	L+2	L+3	L+4
Pd	8.29	0.44	0.83	0.18	4.64	0.18	1.00	0.54	0.82	40.20
Zn	0.09	0.29	0.81	0.02	0.06	0.03	0.21	0.01	0.19	0.04
[Zn]-Zn	47.59	55.09	73.63	2.00	65.01	14.39	83.58	7.37	91.44	29.23
[Fb]	43.18	43.83	24.06	97.08	30.01	84.98	14.74	91.70	7.17	30.37
*t*Bu groups	0.84	0.35	0.67	0.72	0.28	0.41	0.47	0.38	0.39	0.15

a) **[Fb]** and **[Zn]**-Zn are respectively the free base porphyrin and Zn-containing porphyrin chromophores minus the Zn atom.

Computed Electronic Transitions by TDDFT

Table S5. Calculated position of the pure electronic transitions, oscillator strength (f) and major contributions to the transitions for the first 100 transitions of **[Fb]**.

λ(nm)	f	Major contributions (%)	λ(nm)	f	Major contributions (%)
					H-7→L+1 (17%),
1885.104708	0.0153	H→L (99%)	412.6862718	0.0272	H-6→L+1 (56%)
					H-25→L (12%), H-24→L
1011.778494	0.0147	H-1→L (98%)	410.9763214	0.0658	(36%), H-3→L+2 (14%)
		H-3→L (27%),			H-3→L+2 (33%),
939.3388639	0.0329	H-2→L (63%)	407.7460343	0.0037	H-2→L+2 (38%)
					H-7→L+1 (54%),
855.1164676	0.0396	H-4→L (85%)	406.7694772	0.002	H-6→L+1 (29%)
		H-3→L (67%),			
845.0336467	0.1552	H-2→L (25%)	405.598458	0.0196	H-14→L (80%)
		H-7→L (27%),			
772.8189032	0.0179	H-6→L (64%)	398.570536	0.0919	H-15→L (65%)
		H-8→L (46%),			
		H-7→L (26%),			H-16→L (18%),
751.2775655	0.0834	H-5→L (22%)	395.9610904	0.0179	H-4→L+2 (63%)
		H-8→L (33%),			H-16→L (60%),
723.1035614	0.2646	H-5→L (58%)	393.9731066	0.0615	H-4→L+2 (11%)
		H-8→L (17%),			
		H-7→L (40%),			H-19→L (83%), H-18→L
710.7506113	0.0738	H-6→L (29%)	388.7843733	0.0054	(12%)
					H-17→L (51%),
642.1012825	0.0029	H-10→L (94%)	386.9279925	0.1426	H-5→L+2 (14%)
					H-17→L (12%),
					H-6→L+2 (40%),
628.2408748	0.0066	H-9→L (98%)	384.6352815	0.1029	H-5→L+2 (21%)
		H-11→L (22%),			
580.1747152	0.2406	H→L+1 (68%)	383.5524722	0.0058	H-20→L (74%)
		H-11→L (56%),			H-22→L (10%), H-18→L
		H→L+1 (12%),			(11%), H-7→L+2 (35%), H-
528.2180327	0.2888	H→L+2 (25%)	382.4049616	0.0443	6→L+2 (19%)
		H-12→L (40%),			H-22→L (17%), H-21→L
		H-11→L (10%),			(25%), H-18→L (11%), H-
492.1145377	0.1766	H→L+2 (37%)	380.6672909	0.0505	7→L+2 (14%)
					H-21→L (21%),
		H-12→L (54%),			H-8→L+2 (24%),
489.0282674	0.1252	H→L+2 (23%)	378.1939927	0.0875	H-5→L+2 (10%)
					H-21→L (22%),
					H-7→L+2 (13%),
					H-6→L+2 (16%),
476.2728052	0.06	H-1→L+1 (94%)	377.399661	0.0348	H-5→L+2 (28%)
					H-21→L (19%),
471.4733112	0.0127	H-13→L (95%)	375.661546	0.0625	H-8→L+2 (32%),

					H-7→L+2 (15%)
458.1285764	0.1694	H-2→L+1 (85%)	373.7815395	0.0349	H-9→L+1 (85%)
452.2958436	0.0138	H-3→L+1 (88%)	369.7794048	0.0705	H-10→L+1 (68%)
					H-23→L (30%), H→L+3
444.4803063	0.0756	H-4→L+1 (86%)	364.1320939	0.0503	(44%)
		H-22→L (36%),			
		H-18→L (24%),			H-23→L (67%), H→L+3
436.7609703	0.0224	H-15→L (15%)	361.425305	0.0391	(20%)
		H-8→L+1 (50%),			
		H-8→L+2 (14%),			H-25→L (43%), H-24→L
430.4827493	0.0094	H-7→L+1 (14%)	357.0537284	0.0215	(37%)
					H-26→L (61%), H-25→L
428.13404	0.0638	H-1→L+2 (83%)	353.9145257	0.0125	(24%)
		H-3→L+2 (24%),			
		H-2→L+2 (27%),			H-27→L (51%), H-26→L
418.8626238	0.0385	H-1→L+2 (13%)	351.7257777	0.0078	(23%)
		H-8→L+1 (10%),			
414.7987174	0.0177	H-5→L+1 (73%)	350.4234946	0.0087	H-10→L+2 (87%)

Table S6. Calculated position of the pure electronic transitions, oscillator strength (f) and major contributions to the transitions for the first 100 transitions of **[Zn]**.

λ(nm)	**f**	**Major contributions (%)**	**λ(nm)**	**f**	**Major contributions (%)**
2080.257326	0.0136	H→L (100%)	414.4659244	0.0224	H-16→L (79%)
1016.00702	0.0213	H-1→L (93%)	408.9160179	0.0022	H-7→L+1 (82%)
		H-3→L (10%),			H-17→L (57%),
976.7851307	0.0079	H-2→L (82%)	405.9969109	0.0334	H-1→L+2 (17%)
		H-4→L (35%),			
		H-3→L (49%),			H-18→L (35%), H-17→L
915.1412507	0.0219	H-2→L (12%)	402.3473524	0.0572	(33%), H-1→L+2 (24%)
		H-4→L (61%),			H-18→L (38%),
848.3293646	0.1976	H-3→L (35%)	399.0451775	0.0288	H-1→L+2 (41%)
					H-19→L (17%),
816.9159692	0.0257	H-6→L (90%)	397.7649555	0.0419	H-2→L+2 (59%)
					H-20→L (17%), H-19→L
791.6693483	0.2494	H-5→L (90%)	396.3915105	0.0044	(58%)
					H-20→L (78%), H-19→L
745.7195756	0.0433	H-7→L (72%)	393.8104267	0.0052	(18%)
722.9349075	0.017	H-8→L (88%)	391.3244852	0.1853	H-3→L+2 (65%)
					H-21→L (79%),
629.3570388	0.0061	H-9→L (88%)	387.2059233	0.0432	H-4→L+2 (11%)
		H-10→L (63%),			H-22→L (39%),
615.2408527	0.0019	H→L+1 (16%)	385.1490685	0.0894	H-4→L+2 (35%)
					H-22→L (35%),
599.7355809	0.0029	H-11→L (86%)	382.2634786	0.0974	H-4→L+2 (37%)
595.8159289	0.0002	H-12→L (94%)	375.3772038	0.1038	H-6→L+2 (84%)
570.0121219	0.0473	H-13→L (62%),	374.538068	0.0203	H-5→L+2 (82%)

		H→L+1 (33%)			
		H-13→L (30%), H-10→L (20%), H→L+1			H-12→L+1 (14%), H-11→L+1 (18%),
521.7714697	0.5097	(34%)	368.91019	0.0243	H-9→L+1 (44%)
					H-10→L+1 (29%), H-9→L+1 (20%), H→L+3
505.4149307	0.0816	H-14→L (80%)	367.6412544	0.0232	(18%)
483.724149	0.286	H→L+2 (83%)	366.6518901	0.0008	H-23→L (88%)
					H-25→L (16%), H-24→L
469.3849347	0.0316	H-1→L+1 (95%)	363.3743747	0.0095	(69%)
		H-3→L+1 (21%),			H-25→L (69%), H-24→L
459.0785228	0.0644	H-2→L+1 (73%)	362.0162831	0.0128	(24%)
					H-27→L (12%), H-12→L+1 (21%),
		H-3→L+1 (72%),			H-10→L+1 (14%), H→L+3
452.0484801	0.0078	H-2→L+1 (22%)	360.6263428	0.0106	(25%)
442.0240887	0.0388	H-4→L+1 (92%)	359.2262173	0.0903	H-7→L+2 (68%)
429.082321	0.0306	H-5→L+1 (88%)	357.3521736	0.0163	H-26→L (79%)
					H-11→L+1 (10%),
		H-15→L (21%),			H-9→L+1 (14%), H→L+3
423.90364	0.0508	H-6→L+1 (54%)	355.528164	0.0356	(31%)
					H-27→L (33%),
		H-15→L (39%),			H-12→L+1 (25%),
419.0891585	0.0793	H-6→L+1 (32%)	352.666221	0.0324	H-11→L+1 (26%)
					H-27→L (23%), H-13→L+1 (14%),
					H-12→L+1 (21%),
416.4987122	0.0039	H-8→L+1 (67%)	349.3078736	0.0598	H-11→L+1 (18%)

Table S7. Calculated position of the pure electronic transitions, oscillator strength (f) and major contributions to the transitions for the first 100 transitions of **[Fb-Fb]**.

λ(nm)	**f**	**Major contributions (%)**	**λ(nm)**	**f**	**Major contributions (%)**
					H-4→L+3 (11%), H-2→L+5 (33%),
671.1233985	0.1727	H→L (76%)	410.7176488	0.0395	H-1→L+6 (23%)
					H-5→L (29%), H→L+6
659.4858332	0.0077	H→L+1 (67%)	409.5102941	0.0665	(26%)
		H-2→L+1 (22%),			
		H-1→L (51%),			H-5→L+1 (43%), H→L+5
626.2417246	0.2777	H→L+2 (12%)	403.4077459	0.3658	(32%)
		H-2→L (48%),			
		H-1→L+1 (24%),			H-7→L (42%), H-6→L+1
621.0345454	0.0071	H→L+1 (10%)	392.0793645	0.0002	(34%)
		H-3→L (32%),			
		H-2→L (16%),			H-7→L+1 (38%), H-6→L
589.8070341	0.0007	H-1→L+1 (34%),	391.5840334	0.0078	(52%)

		H→L+1 (11%)			
585.6281547	0.0009	H-2→L+1 (60%), H-1→L (36%)	388.991738	0.0143	H-20→L+4 (14%), H-12→L+4 (15%), H→L+6 (25%)
582.1633875	0.0004	H-3→L (38%), H-2→L (19%), H-1→L+1 (29%)	383.1376287	0.0443	H-2→L+6 (32%), H-1→L+5 (39%), H-1→L+6 (13%)
578.226549	0.1031	H-3→L+1 (66%), H→L (10%)	382.9719424	0.0145	H-2→L+5 (28%), H-2→L+6 (12%), H-1→L+6 (36%)
524.6195432	0.3358	H→L+2 (22%), H→L+4 (57%)	382.1221002	0.0051	H-12→L (48%)
515.0306843	1	H→L+2 (61%), H→L+4 (20%)	381.9102287	0.5795	H-4→L+2 (35%), H-2→L+6 (17%)
500.1546518	0.0234	H-2→L+2 (32%), H→L+3 (37%)	380.433681	0.3875	H-9→L+1 (19%), H-8→L (28%), H-4→L+2 (15%)
490.7510158	0.5459	H-4→L (15%), H-3→L+1 (22%), H-1→L+2 (50%)	379.8625468	0.0053	H-9→L (36%), H-8→L+1 (28%)
486.4762483	0.0334	H-3→L+2 (15%), H-2→L+2 (21%), H→L+3 (40%)	379.061198	0.0438	H-4→L+3 (18%), H-3→L+5 (33%)
478.1647446	0.0088	H-2→L+2 (21%), H-1→L+3 (66%)	378.6791382	0.0016	H-12→L+1 (43%), H-9→L+1 (10%), H-8→L (14%)
477.4466137	0.0649	H-2→L+3 (67%), H-1→L+2 (21%)	374.6625669	0.039	H-11→L+1 (21%), H-10→L (33%), H-3→L+6 (27%)
457.655076	0.0006	H-4→L+1 (17%), H-3→L+2 (53%)	374.617285	0.009	H-11→L (14%), H-10→L+1 (10%), H-4→L+3 (21%), H-3→L+5 (15%)
455.888133	0.2256	H-4→L (31%), H-3→L+3 (43%)	372.6468595	0.2654	H-14→L+1 (11%), H-13→L (13%), H-3→L+6 (50%)
445.4704536	1.3564	H-4→L (29%), H-3→L+3 (41%)	372.3782449	0.0602	H-11→L (22%), H-10→L+1 (18%), H-3→L+5 (25%)
438.5685767	0.1565	H-4→L+1 (35%), H-3→L+2 (14%), H→L+6 (11%)	371.0742746	0.0942	H-21→L+4 (18%), H-4→L+4 (33%)
425.1245942	0.0032	H-3→L+4 (59%), H-2→L+4 (27%)	371.0187528	0.0554	H-14→L (21%), H-13→L+1 (25%)
423.5126785	0.0259	H-1→L+4 (91%)	370.9410503	0.1177	H-14→L (14%), H-14→L+1 (19%), H-13→L (19%)
419.3301202	0.0008	H-3→L+4 (18%), H-2→L+4 (54%)	367.3798051	0.023	H-20→L+1 (21%), H-15→L (55%)
417.1854256	0.0202	H-5→L (35%), H-4→L+1 (15%), H-2→L+4 (14%),	366.0889262	0.0004	H-20→L (31%), H-19→L (15%), H-15→L+1 (43%)

		H→L+6 (14%)			
415.9118975	0.3751	H-5→L+1 (17%), H→L+5 (47%)	363.5235344	0.0011	H-18→L (25%), H-16→L (28%), H-16→L+1 (24%)
412.6450664	0.0697	H-5→L+1 (25%), H-4→L+2 (15%), H-2→L+6 (18%), H-1→L+5 (28%)	363.4595938	0.0015	H-18→L (16%), H-18→L+1 (12%), H-17→L (23%), H-17→L+1 (17%), H-16→L (14%)

Table S8. Calculated position of the pure electronic transitions, oscillator strength (f) and major contributions to the transitions for the first 100 transitions of **[Zn-Zn]**.

λ(nm)	**f**	**Major contributions (%)**	**λ(nm)**	**f**	**Major contributions (%)**
659.4156826	0.1928	H→L (90%)	402.922676	0.0011	H-19→L+1 (17%), H-18→L (12%), H-13→L+1 (19%), H-12→L (26%)
645.6120425	0.001	H→L+1 (85%)	402.8572155	0.0008	H-19→L (19%), H-18→L+1 (11%), H-13→L (23%), H-12→L+1 (21%)
611.3576757	0.0289	H-2→L+1 (21%), H-1→L (49%)	399.327933	0.3324	H-5→L+1 (43%), H→L+5 (33%)
611.1768542	0.363	H-3→L+1 (14%), H-2→L (54%), H→L+2 (12%)	396.8355684	0.1337	H-4→L+2 (22%), H-3→L+6 (11%), H-2→L+5 (32%)
587.1257122	0.0051	H-3→L (36%), H-2→L+1 (11%), H-1→L (30%)	395.1534187	0.0011	H-4→L+3 (14%), H-3→L+5 (17%), H-2→L+6 (27%), H-1→L+5 (18%)
582.8749783	0.0853	H-1→L+1 (78%)	387.7993702	0.0155	H-25→L+4 (14%), H-12→L+4 (16%), H→L+6 (32%)
558.1315235	0.0002	H-3→L (38%), H-2→L+1 (54%)	382.9364569	0.029	H-7→L (15%), H-7→L+1 (21%), H-6→L (39%)
554.1897758	0.0223	H-3→L+1 (59%), H-2→L (32%)	382.5937686	0	H-7→L (32%), H-6→L (10%), H-6→L+1 (30%)
527.2072826	0.0482	H-4→L+4 (15%), H→L+4 (74%)	379.5369536	0.0008	H-10→L (10%), H-9→L+1 (11%), H-8→L (26%)
496.6087344	1.525	H→L+2 (77%)	379.3279383	0.0056	H-9→L (12%), H-8→L+1 (13%), H-1→L+5 (25%)
476.1264848	0.0001	H-1→L+2 (35%), H→L+3 (53%)	378.0325537	0.0469	H-9→L (10%), H-1→L+5 (36%)
471.4912406	0.0197	H-4→L+1 (29%), H-3→L+2 (18%), H-2→L+3 (13%), H→L+3 (16%)	377.3537151	0.1068	H-24→L+4 (12%), H-4→L+4 (41%), H→L+4 (14%)

470.8824027	0.3559	H-4→L (42%), H-2→L+2 (31%)	376.5400329	0.0482	H-10→L (20%), H-9→L+1 (11%), H-8→L (15%), H-1→L+6 (10%)
453.7857281	0.1988	H-4→L (24%), H-2→L+2 (40%), H-1→L+3 (21%)	376.2886177	0.0106	H-11→L (20%), H-10→L+1 (13%), H-9→L (21%), H-8→L+1 (14%)
447.6902457	0.8459	H-4→L (18%), H-1→L+3 (59%)	375.8095742	0.2852	H-1→L+6 (54%)
445.9832253	0.0279	H-4→L+1 (36%), H-3→L+2 (31%)	373.3763074	0.0015	H-25→L (18%), H-19→L+1 (12%), H-18→L (13%), H-12→L (36%)
443.2567182	0.0019	H-2→L+3 (55%), H-1→L+2 (23%)	372.0206939	0.6007	H-4→L+2 (30%), H-2→L+5 (25%)
440.6259743	0.055	H-3→L+2 (35%), H-2→L+3 (12%), H-1→L+2 (16%)	370.1326586	0.0411	H-25→L+1 (11%), H-19→L (17%), H-18→L+1 (10%), H-12→L+1 (30%)
435.7172259	0.5881	H-3→L+3 (73%), H-2→L+2 (14%)	368.4278398	0.0024	H-15→L (18%), H-14→L+1 (17%), H-2→L+6 (18%)
431.741953	0.0016	H-3→L+4 (12%), H-1→L+4 (80%)	367.6630587	0.1045	H-15→L+1 (11%), H-14→L (18%), H-10→L (11%), H-4→L+2 (10%)
421.4110215	0.0002	H-2→L+4 (92%)	366.9991908	0.006	H-3→L+5 (47%), H-2→L+6 (34%)
411.7679729	0.0074	H-5→L (53%), H-4→L+1 (11%), H-3→L+4 (13%), H→L+6 (10%)	365.8080921	0.002	H-4→L+3 (42%)
411.4946453	0.0022	H-5→L (10%), H-3→L+4 (69%), H-1→L+4 (12%)	365.6786216	0.1277	H-3→L+6 (72%), H-2→L+5 (18%)
409.3345328	0.2817	H-5→L+1 (38%), H→L+5 (42%)	365.0756357	0.0021	H-19→L (10%), H-15→L+1 (12%), H-13→L (37%)
407.0098373	0.0496	H-25→L+4 (15%), H-12→L+4 (17%), H-5→L (12%), H→L+6 (27%)	364.0786299	0.012	H-18→L (11%), H-17→L (10%), H-15→L (17%), H-13→L+1 (18%)

Table S9. Calculated position of the pure electronic transitions, oscillator strength (f) and major contributions to the transitions for the first 100 transitions of **[Fb-Zn]**.

λ(nm)	f	Major contributions (%)	λ(nm)	f	Major contributions (%)
669.059072	0.1282	HOMO→LUMO (74%)	407.5851824	0.1034	H-5→L+1 (29%), HOMO→L+6 (30%)
646.757103	0.0732	HOMO→L+1 (82%)	403.0274571	0.0012	H-18→L+1 (26%), H-11→LUMO (10%), H-11→L+1 (40%)
623.0631521	0.1681	H-1→LUMO (64%)	400.2948912	0.261	H-5→L+1 (41%), HOMO→L+5 (23%)
610.6951859	0.0919	H-2→LUMO (35%), H-2→L+1 (33%), HOMO→L+3 (12%)	395.2038016	0.0574	H-4→L+3 (15%), H-3→L+6 (10%), H-2→L+5 (12%), H-2→L+6 (37%)
595.5583468	0.1119	H-3→LUMO (34%), H-2→LUMO (16%), H-2→L+1 (17%)	391.6335101	0.0086	H-6→LUMO (81%)
572.5919579	0.0127	H-3→LUMO (20%), H-3→L+1 (11%), H-2→LUMO (11%), H-2→L+1 (15%), H-1→L+1 (35%)	388.4798265	0.0828	H-11→L+4 (11%), HOMO→L+6 (32%)
569.3054304	0.0043	H-3→LUMO (13%), H-2→L+1 (20%), H-1→L+1 (53%)	382.9364569	0.0051	H-7→LUMO (17%), H-7→L+1 (61%)
565.5142157	0.037	H-3→L+1 (52%), H-2→LUMO (27%)	382.0279061	0.1187	H-11→LUMO (10%), H-3→L+5 (10%), H-2→L+5 (19%)
525.5981035	0.1593	H-4→L+4 (12%), HOMO→L+2 (11%), HOMO→L+4 (64%)	380.7374298	0.123	H-15→LUMO (10%), H-14→LUMO (13%), H-11→LUMO (20%)
512.3490088	0.8171	HOMO→L+2 (74%), HOMO→L+4 (10%)	379.7927298	0.0375	H-9→LUMO (47%), H-2→L+5 (10%)
492.4663832	0.3043	H-4→LUMO (18%), H-3→LUMO (12%), H-1→L+2 (46%)	379.5485723	0.186	H-9→LUMO (26%), H-8→L+1 (12%), H-4→L+2 (16%)
479.7002888	0.6537	H-2→L+2 (41%), HOMO→L+3 (41%)	378.1363201	0.4172	H-8→L+1 (17%), H-4→L+2 (15%), H-2→L+5 (16%)
470.3464971	0.1851	H-4→L+1 (15%), H-3→L+2 (17%), H-2→L+2 (18%), HOMO→L+3 (15%)	376.4371406	0.0153	H-10→L+1 (34%), H-8→L+1 (26%)
464.0615961	0.0449	H-4→LUMO (16%), H-2→L+2 (21%), H-2→L+3 (35%)	374.0521832	0.0118	H-12→LUMO (26%), H-3→L+5 (26%), H-2→L+5 (15%)
458.9086007	0.0797	H-4→LUMO (16%), H-3→L+2 (39%),	373.5788135	0.0034	H-4→L+4 (30%)

		H-1→L+3 (11%)			
					H-12→LUMO (24%),
					H-3→L+5 (10%),
450.7501514	0.0633	H-1→L+3 (80%)	373.2751367	0.042	H-1→L+6 (28%)
		H-4→LUMO (18%),			H-3→L+5 (15%),
		H-4→L+1 (22%),			H-2→L+6 (11%),
447.1574157	0.5091	H-2→L+3 (24%)	372.8261514	0.051	H-1→L+6 (52%)
		H-4→LUMO (12%),			
		H-4→L+1 (23%),			H-18→L+1 (17%),
440.4224953	0.3975	H-3→L+2 (10%)	371.296528	0.0101	H-11→L+1 (21%)
		H-3→L+3 (59%),			H-14→LUMO (10%),
437.4081377	0.5312	H-2→L+3 (12%)	370.8966634	0.1074	H-3→L+6 (24%)
		H-3→L+4 (30%),			H-15→LUMO (32%),
		H-2→L+4 (43%),			H-14→LUMO (24%),
428.1488246	0.0041	H-1→L+4 (12%)	370.4533783	0.1464	H-12→LUMO (10%)
		H-3→L+4 (16%),			H-13→L+1 (20%),
420.425014	0.0111	H-1→L+4 (75%)	367.4560228	0.047	H-3→L+6 (21%)
					H-15→LUMO (14%),
		H-5→LUMO (44%),			H-14→LUMO (18%),
417.9871102	0.0713	HOMO→L+5 (24%)	366.6410476	0.0147	H-11→LUMO (11%)
		H-3→L+4 (40%),			H-4→L+3 (31%),
415.326734	0.0004	H-2→L+4 (47%)	365.9808621	0.1605	H-3→L+6 (24%)
		H-4→L+2 (18%),			H-15→L+1 (14%),
410.8265239	0.0538	H-1→L+5 (58%)	364.2069697	0.0161	H-13→L+1 (14%)
		H-5→LUMO (30%),			H-19→LUMO (26%),
409.7674477	0.2264	HOMO→L+5 (31%)	362.9701289	0.0031	H-17→LUMO (58%)

Graphs representing the computed oscillator strengths vs the positions of the electronic transitions for [Fb-Zn], [Zn-Zn] and [Fb-Fb].

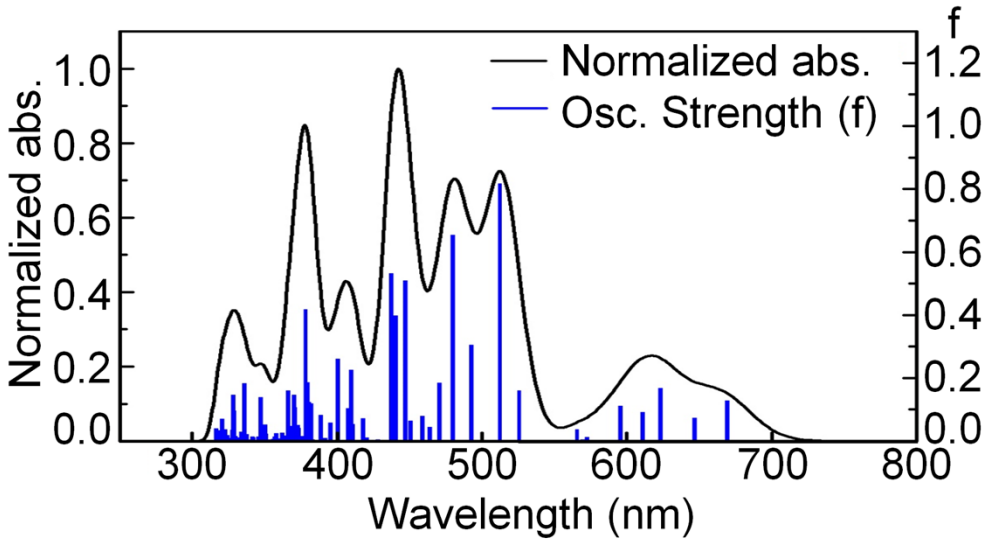

Figure S21. Bar graph reporting the oscillator strengths (f) as a function of the positions of the electronic transition (blue). The black trace is the same but applying a thickness of 1000 cm^{-1} to each bar.

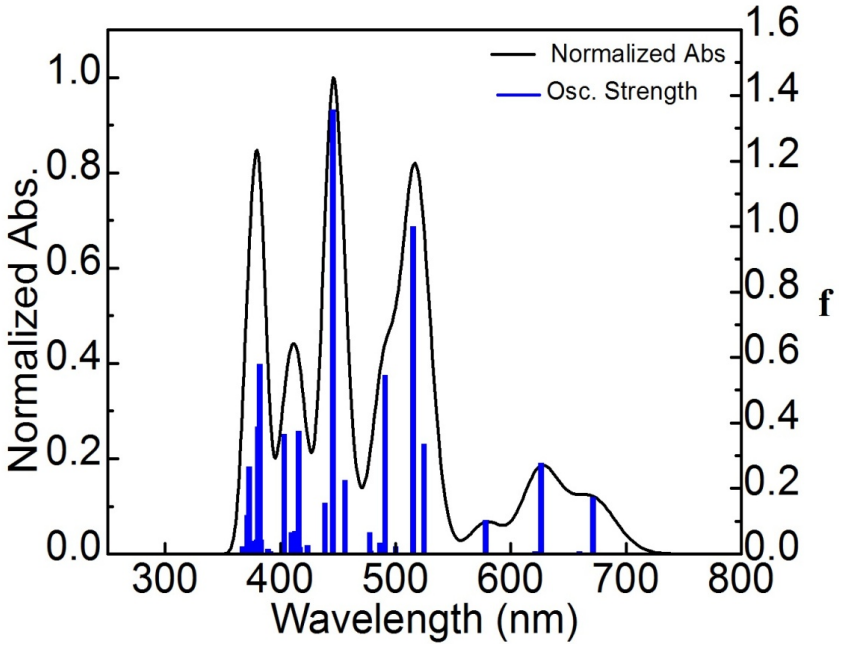

Figure S22. Bar graph showing the oscillator strength, f, as a function of the calculated positions of the electronic transitions (blue) for **[Fb-Fb]**. The black line is the generated spectrum when assigning 1000 cm^{-1} for each transition.

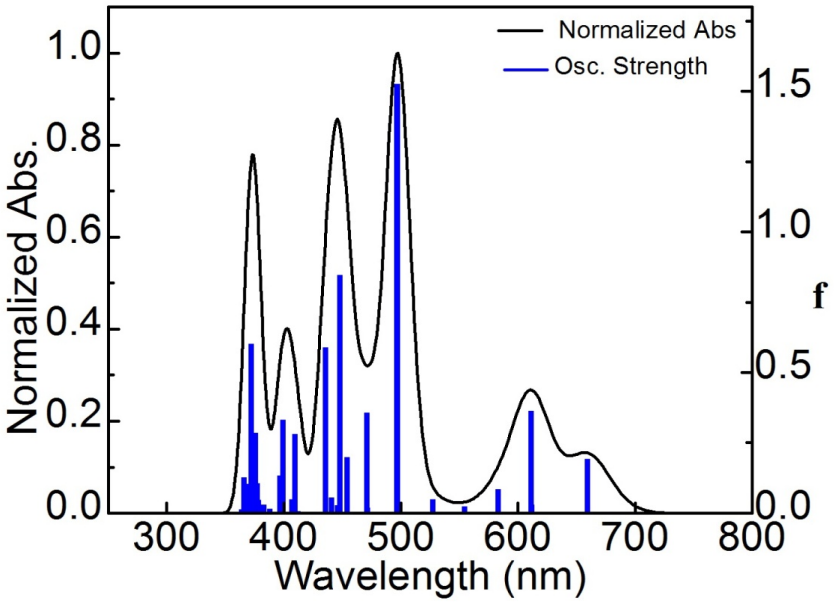

Figure S23. Bar graph showing the oscillator strength, f, as a function of the calculated positions of the electronic transitions (blue) for **[Zn-Zn]**. The black line is the generated spectrum when assigning 1000 cm^{-1} for each transition.

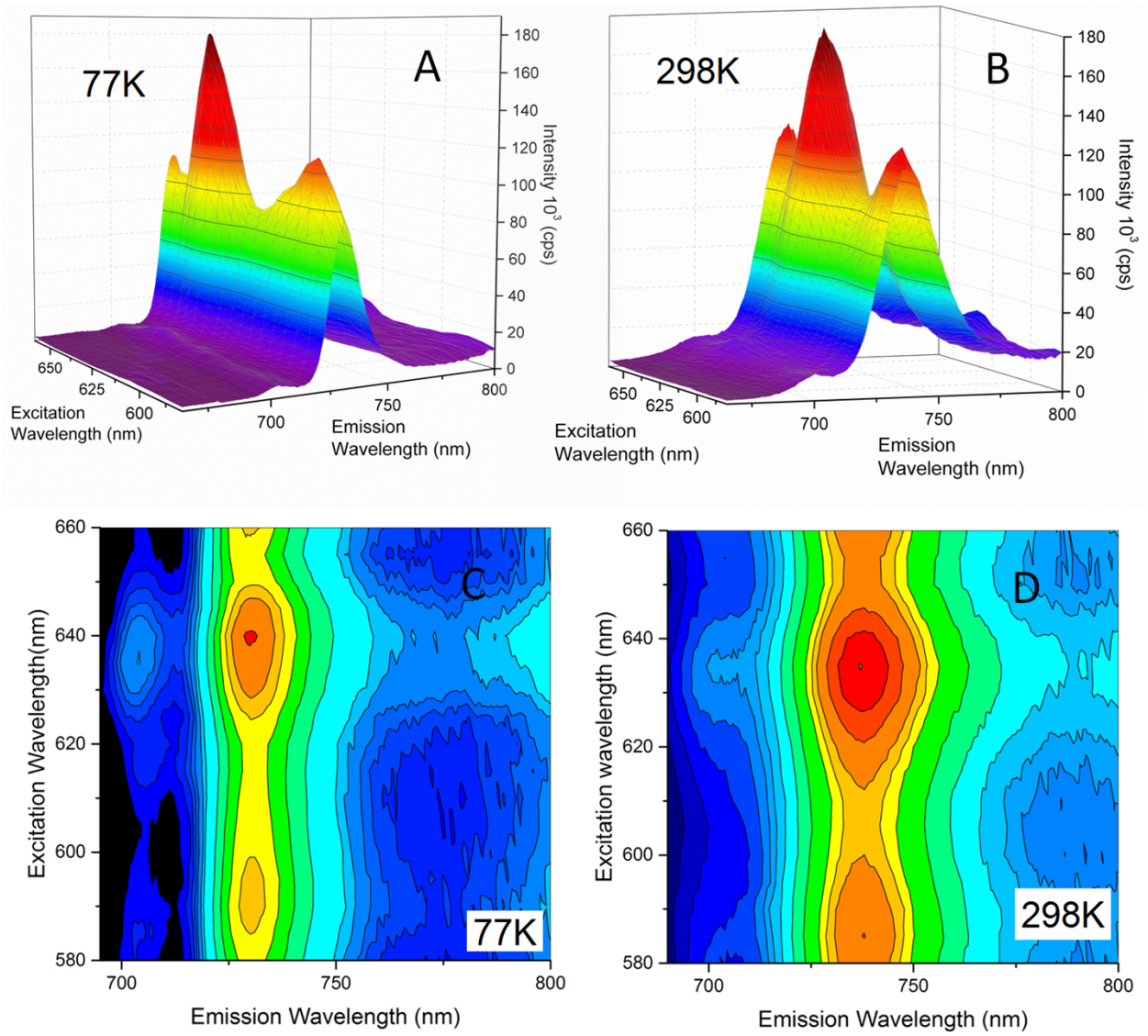

Figure S24. 3D (top) and contour maps (bottom) showing the fluorescence spectra of **[Fb-Zn]** in 2-MeTHF at 77 (A, C) and 298 K (B, D).

The total fluorescence intensity for both chromophores (see the **[Zn]**- (~700 nm) and **[Fb]**- (~735 nm) bands) follows the absorption spectrum of **[Fb-Zn]** indicating efficient energy transfer. The relative intensity of the **[Zn]**-fluorescence *vs* **[Fb]**-fluorescence is smaller at 77 K.

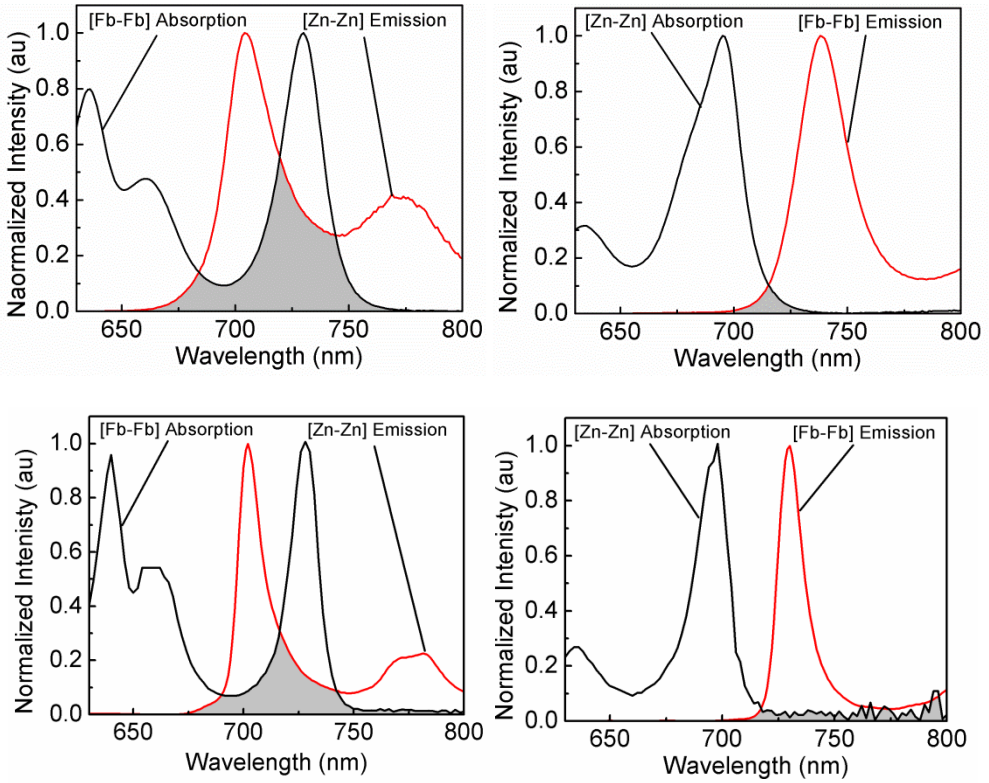

Figure S25. Spectral overlaps using the models **[Zn-Zn]** and **[Fb-Fb]** for examining the forward **[Zn]*→[Fb]** (left) and the back **[Fb]*→[Zn]** energy transfers (right) at 298 (top) and at 77 K (bottom).

The Förster and Dexter equations are as follow :

$$k_{Förster} = \frac{\Phi_F^o(D)\kappa^2}{\tau_F^o(D)r^6}\cdot\left(\frac{9000(ln10)}{128\pi^5 N_a n^4}\right)\cdot J \quad or \quad k_{Förster} \cong 8.785\times10^{-25}\cdot\left(\frac{k_F^o(D)\kappa^2}{r^6 n^4}\right)\cdot J$$

$$and \quad k_{Dexter} = K\cdot J\cdot e^{\left(\frac{-2r}{L}\right)}$$

$$J(M^{-1}cm^3) = \frac{\int_0^\infty \frac{F_D(\nu)\varepsilon_A(\nu)}{\nu^4}d\nu}{\int_0^\infty F_D(\nu)d\nu} = \int_0^\infty \frac{F_D^*(\nu)\varepsilon_A(\nu)}{\nu^4}d\nu$$

where the J-integral is given by

and $\Phi_F°$ and $\tau_F°$ are respectively the fluorescence quantum yield and lifetime of the donor in the absence of an acceptor ([Zn-Zn] for example), κ^2 is a reorganizational parameter (relationship

between the transition moments of the donor and the acceptor chromophores), r is the center-to-center distance between the donor and the acceptor, n is the refractive index of the medium, N_a is the Avogadro's number, K is an experimental value, L is the van der Waals radius of the donor, F_D is the fluorescence intensity as a function of ν (the frequency) and ε_A is the absorptivity of the acceptor also at different frequency.

Evidence for the heavy atom effect in **[Fb-Fb]**, **[Zn-Zn]** and **[Fb-Zn]**:

In our previous work on structurally related dimers placed below, in which no electronic communication took place (ref. 8: M. Abdelhameed, P.-L. Karsenti, A. Langlois, J.-F. Lefebvre, S. Richeter, R. Ruppert and P. D. Harvey, *Chemistry, a European Journal*, **2014**, in press. DOI: 10.1002/chem.201403146.), we showed that the t_F values in the monomers and dimers did not change very much. This means that both the internal conversion rate, k_{ic}, and the inter-system crossing rate constants, k_{isc}, were not affected upon this modification (see Table).

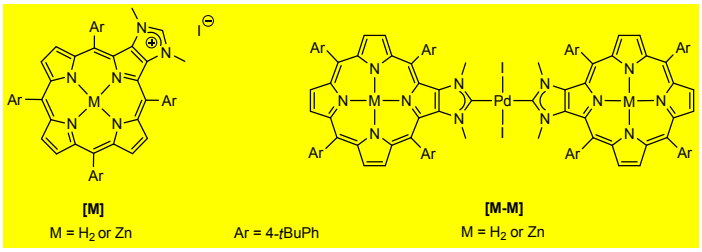

Structurally related dimers to the dimers and dyads investigated in this work.

***Table S10*. Photophysical data of [Zn], [Fb], [Zn-Zn], [Fb-Fb] and [Fb-Zn] above in 2MeTHF.**

	298K		77K	
	λ_{em}[a] (nm)	τ_F (ns)[b][c] (cont. %)	λ_{em}[a] (nm)	τ_F (ns)[b][c] (cont. %)
[Zn]	637	0.57±0.10	633	0.88±0.10
[Zn-Zn]	630	0.65±0.10	618	1.07±0.10
[Fb-Zn]	675	0.130±0.001(D) 4.55±0.10(A)	667	0.081±0.001(D) 0.277±0.001(D) 4.88±0.10(A)
[Fb-Fb]	674	4.43±0.64	667	5.74±0.10
[Fb]	672	5.85±0.10	665	6.02±0.10

[a] λ_{exc} = 430 nm and λ_{em}(nm) is the monitoring wavelength. [b] λ_{exc} = 430 nm; the detection limit is 100 ps unless indicated otherwise. D = donor; A = acceptor.

Moreover, the t_F values of a series of cofacial bisporphyrins placed below where no heavy atom is present were analyzed by one of us. See Camus, J.-M.; Aly, S. M.; Stern, C.; Guilard, R.; Harvey, P. D. Chem. Commun. 2011, 47, 8817-8819. The t_F values do not change within the uncertainties and so k_{ic} is relatively constant. Because of these facts, the presence of heavy atom is unambiguously operating in **[Fb-Fb]**, **[Zn-Zn]** and **[Fb-Zn]**

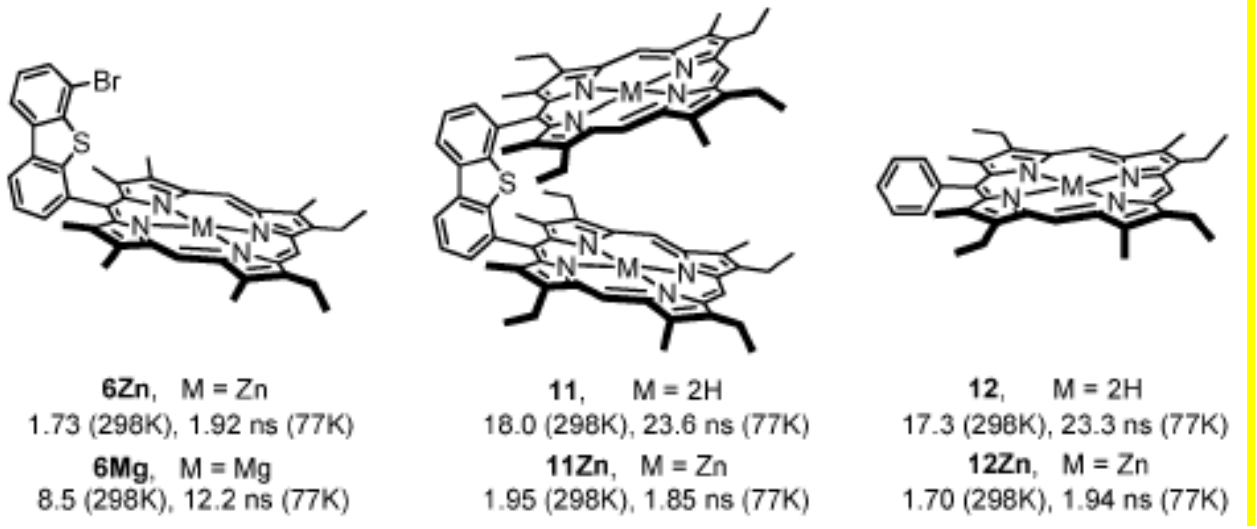

6Zn, M = Zn
1.73 (298K), 1.92 ns (77K)
6Mg, M = Mg
8.5 (298K), 12.2 ns (77K)

11, M = 2H
18.0 (298K), 23.6 ns (77K)
11Zn, M = Zn
1.95 (298K), 1.85 ns (77K)

12, M = 2H
17.3 (298K), 23.3 ns (77K)
12Zn, M = Zn
1.70 (298K), 1.94 ns (77K)

Structures of mono-porphyrin and their cofacial dimers.

References

[1] S. Richeter, C. Jeandon, J.-P. Gisselbrecht, R. Ruppert, H. J. Callot, *J. Am. Chem. Soc.* **2002**, *124*, 6168-6179.

[2] F. Nifiatis, J. C. Athas, K. D. D. Gunaratne, Y. Gurung, K. M. Monette, P. J. Shivokevich; *The Open Spectroscopy Journal* **2011**, *5*, 1-12.

[3] M. J. Frisch *et al*. Gaussian, Inc., Wallingford CT, **2004**.

[4] P. Hohenberg, W. Kohn, *Phys. Rev.* **1964**, *136*, B864-871.

[5] W. Kohn, L. J. Sham, *Phys. Rev.* **1965**, *140*, A1133-1138.

[6] R.G. Parr, W. Yang, Density-functional theory of atoms and molecules, Oxford Univ. Press: Oxford, **1989**.

[7] D. R. Salahub, M. C. Zerner, The Challenge of d and f Electrons, Amer. Chem. Soc. Washington, D.C. **1989**.

[8] R. Bauernschmitt, X. Ahlrichs, *Chem. Phys. Lett.* **1996**, *256*, 454-464.

[9] M. E. Casida, C. Jamorski, K. C. Casida, D. R Salahub, *J. Chem. Phys.* **1998**, *108*, 4439-4449.

[10] R. E. Stratmann, G. E. Scuseria, M. J. Frisch, *J. Chem. Phys.* **1998**, *109*, 8218-8224.

[11] C. Lee, W. Yang, R. G. Parr, *Phys. Rev. B* **1988**, *37*, 785-789.

[12] B. Miehlich, A. Savin, H. Stoll, H. Preuss, *Chem. Phys. Lett.* **1989**, *157*, 200-206.

[13] A. D. Becke, *J. Chem. Phys.* **1993**, *98*, 5648-5652.

[14] R. Ditchfield, W. J. Hehre, J. A. Pople, *J. Chem. Phys.* **1971**, *54*, 724-728.

[15] W. J. Hehre, R. Ditchfield, J. A. Pople, *J. Chem. Phys.* **1972**, *56*, 2257-2261.

[16] P. C. Hariharan, J. A. Pople, *Mol. Phys.* **1974**, *27*, 209-214.

[17] M. S. Gordon, *Chem. Phys. Lett.* **1980**, *76*, 163-168.

[18] P. C. Hariharan, J. A. Pople, *Theo. Chim. Acta* **1973**, *28*, 213-222.

[19] J.-P. Blaudeau, M. P. McGrath, L. A. Curtiss, L. Radom, *J. Chem. Phys.* **1997**, *107*, 5016-5021.

[20] M. M. Francl, W. J. Pietro, W. J. Hehre, J. S. Binkley, D. J. DeFrees, J. A. Pople, M. S. Gordon, *J. Chem. Phys.* **1982**, *77*, 3654-3665.

[21] J. S. Binkley, J. A. Pople, W. J. Hehre, *J. Am. Chem. Soc.* **1980**, *102*, 939-947.

[22] M. S. Gordon, J. S. Binkley, J. A. Pople, W. J. Pietro, W. J. Hehre, *J. Am. Chem. Soc.* **1982**, *104*, 2797-2803.

[23] W. J. Pietro, M. M. Francl, W. J. Hehre, D. J. Defrees, J. A. Pople, J. S. Binkley, *J. Am. Chem. Soc.* **1982**, *104*, 5039-5048.

[24] K. D. Dobbs, W. J. Hehre, *J. Comp. Chem.* **1986**, *7*, 359-378.

[25] K. D. Dobbs, W. J. Hehre, *J. Comp. Chem.* **1987**, *8*, 861-879.

[26] K. D. Dobbs, W. J. Hehre, *J. Comp. Chem.* **1987**, *8*, 880-893.

[27] N. Godbout, D. R. Salahub, J. Andzelm, E. Wimmer. *Can. J. Chem.* **1992**, *70*, 560-571.

[28] SBKJC ECP EMSL Basis Set Exchange Library.

[29] W. J. Stevens, M. Krauss, H. Basch, P. G. Jasien, *Can. J. Chem.* **1992**, *70*, 612-630.

[30] N. M. O'Boyle, A. L.Tenderholt, K. M. Langner, *J. Comp. Chem.* **2008**, *29*, 839-845.